# From evaporated seawater to uranium-mineralizing brines: Isotopic and trace element study of quartz-dolomite veins in the Athabasca system

Antonin Richard, Philippe Boulvais, Julien Mercadier, Marie-Christine Boiron, Michel Cathelineau, Michel Cuney, Christian France-Lanord

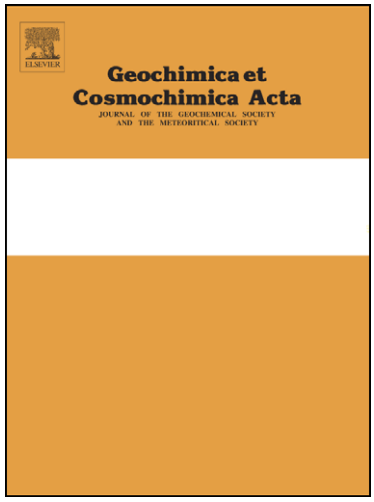


# From evaporated seawater to uranium-mineralizing brines: Isotopic and trace element study of quartz-dolomite veins in the Athabasca system

Antonin Richard, Philippe Boulvais, Julien Mercadier, Marie-Christine Boiron, Michel Cathelineau, Michel Cuney, Christian France-Lanord

PII: S0016-7037(13)00151-8
DOI: http://dx.doi.org/10.1016/j.gca.2013.03.009
Reference: GCA 8189

To appear in: *Geochimica et Cosmochimica Acta*

Received Date: 8 August 2012
Accepted Date: 8 March 2013

Please cite this article as: Richard, A., Boulvais, P., Mercadier, J., Boiron, M-C., Cathelineau, M., Cuney, M., France-Lanord, C., From evaporated seawater to uranium-mineralizing brines: Isotopic and trace element study of quartz-dolomite veins in the Athabasca system, *Geochimica et Cosmochimica Acta* (2013), doi: http://dx.doi.org/10.1016/j.gca.2013.03.009

# From evaporated seawater to uranium-mineralizing brines: Isotopic and trace element study of quartz-dolomite veins in the Athabasca system

Antonin Richard [a,b,*], Philippe Boulvais [c], Julien Mercadier [a], Marie-Christine Boiron [a], Michel Cathelineau [a], Michel Cuney [a], Christian France-Lanord [d]

[a] *GéoRessources, Université de Lorraine, CNRS, CREGU, Boulevard des Aiguillettes, BP 70239, F-54506, Vandoeuvre-lès-Nancy, France*

[b] *Geological Survey of Finland, P.O. Box 96, FI-02151 Espoo, Finland*

[c] *Géosciences UMR 6118, CNRS - Université de Rennes 1, Campus de Beaulieu, 35042 Rennes Cedex, France.*

[d] *Centre de Recherche Pétrographique et Géochimique, Université de Lorraine, CNRS, 15 rue Notre Dame des Pauvres, 54501 Vandoeuvre-lès-Nancy, France*

* Corresponding author: Antonin Richard, Geological Survey of Finland, P.O. Box 96, FI-02151 Espoo, Finland

Phone : +358504363655

Fax : +358295032901

Mail : antonin.richard@gtk.fi

**Abstract**

Stable isotope (O, H, C), radiogenic isotope (Sr, Nd) and trace element analyses have been applied to quartz-dolomite veins and their uranium(U)-bearing fluid inclusions associated with Proterozoic unconformity-related $UO_2$ (uraninite) ores in the Athabasca Basin (Canada) in order to trace the evolution of pristine evaporated seawater towards U-mineralizing brines during their migration through sediments and basement rocks.

Fluid inclusion data show that quartz and dolomite have precipitated from brines of comparable chemistry (excepted for relatively small amounts of $CO_2$ found in dolomite-hosted fluid inclusions). However, $\delta^{18}O$ values of quartz veins ($\delta^{18}O$ = 11‰ to 18‰) and dolomite veins ($\delta^{18}O$ = 13‰ to 24‰) clearly indicate isotopic disequilibrium between quartz and dolomite. Hence, it is inferred that this isotopic disequilibrium primarily reflects a decrease in temperature between the quartz stage (~180°C) and the dolomite stage (~120°C). The $\delta^{13}C$ values of $CO_2$ dissolved in dolomite-hosted fluid inclusions ($\delta^{13}C$ = -30‰ to -4‰) and the $\delta^{13}C$ values of dolomite ($\delta^{13}C$ = -23.5‰ to -3.5‰) indicate that the $CO_2$ dissolved in the mineralizing brines originated from brine-graphite interactions in the basement. The resulting slight increase in the fluid partial pressure of ($pCO_2$) content may have triggered dolomite precipitation instead of quartz.

$\delta^{18}O$ values of quartz veins and previously published $\delta^{18}O$ values of the main alteration minerals around the U-ores (illite, chlorite and tourmaline) show that quartz and alteration minerals were isotopically equilibrated with the same fluid at ~180°C. The REE concentrations in dolomite produce PAAS-normalized patterns that show some similarities with that of $UO_2$ and are clearly distinct from that of the other main REE-bearing minerals in these environments (monazite, zircon and aluminum phosphate-sulfate (APS) minerals). The radiogenic isotope compositions of dolomite ($^{87}Sr/^{86}Sr_i$ = 0.7053 to 0.7161 and $\varepsilon_{Nd}(t)$ = -8.8 to

-20.3) differ from one deposit to another, reflecting both heterogeneity in the basement geology and variable preservation of the original composition of brines. The previously published $^{87}Sr/^{86}Sr_i$ and $\varepsilon_{Nd}(t)$ values of $UO_2$ compare with the most evolved dolomites, i.e. dolomites precipitated from brines that exchanged the most with the basement. This reinforces a close genetic link between dolomites and $UO_2$ deposition and implies that $UO_2$ deposition occurred in a cooling system during the transition from quartz to dolomite formation.

The calculated $\delta^{18}O$ values of the mineralizing brines ($\delta^{18}O$ = -1‰ to 8‰ and $\delta D$ = -150‰ to -50‰) are considerably shifted from that of their theoretical original values acquired during evaporation of seawater ($\delta^{18}O$ = ~ -3‰ and $\delta D$ = ~ -40‰). The positive $\delta^{18}O$ shift is explained by protracted fluid-rock interaction within the basin and basement rocks. The negative $\delta D$ shift is attributed to incomplete mixing between the U-mineralizing brines and low $\delta D$ water. This low $\delta D$ water was likely produced during the abiogenic synthesis of bitumen by Fisher-Tropsch-like reactions involving $CO_2$ derived from brine-graphite interaction in the basement, and radiolytic $H_2$. The resulting low $\delta D$ brines have been equilibrated with alteration minerals. This may explain why some alteration minerals yield anomalously low $\delta D$ values whose significance has long been debated.

## 1. INTRODUCTION

A variety of mineral deposits are thought to have formed from brines derived from seawater evaporation (e.g. Kesler et al. 1995; Muchez et al. 2005; Essarraj et al. 2005; Richard et al., 2011). Due to their high ionic strength, pristine evaporated seawaters are highly reactive fluids which may scavenge metals in the rocks through which they circulate and ultimately form mineral deposits. Hence, tracing brine-rock interaction in such brine-related systems could greatly help deciphering some key aspects of the ore-forming processes.

The Proterozoic Athabasca Basin (Saskatchewan, Canada) hosts numerous 'unconformity-related' uranium (U) deposits located close to the interface between the Archean to Paleoproterozoic crystalline basement, the late-Paleoproterozoic sedimentary cover and reactivated basement-rooted faults (Jefferson et al., 2007; Kyser and Cuney, 2008). The ~1.5 to ~1.0 Ga $UO_2$ (uraninite) ores document protracted and large-scale circulation of basin-derived oxidizing U-rich brines at the basement/cover interface (e.g. Hoeve and Sibbald, 1978; Kotzer and Kyser, 1995; Fayek and Kyser, 1997; Kyser et al., 2000; Derome et al., 2005; Boiron et al., 2010; Richard et al., 2012).

The origin of the basinal brines has been investigated based on coupled Cl/Br and $\delta^{37}Cl$ composition of fluid inclusions and $\delta^{11}B$ composition of Mg-tourmaline (dravite) associated to U ores (Richard et al., 2011; Mercadier et al., 2012). These studies have shown that the mineralizing brines originate from evaporation of seawater beyond halite saturation, and reached a salt content of ~30 wt% before percolating through the sedimentary pile and the crystalline basement. Since the primary origin of brines is known, stable isotope (O, H, C), radiogenic isotope (Sr, Nd) and trace element analyses can be applied to quartz-dolomite veins and their fluid inclusions associated with U-ores, in order to highlight the processes occurring during the evolution of evaporated-seawater towards U-mineralizing brines. While

few data exist in the literature regarding the stable isotope composition (O, H, C) of quartz and dolomite veins and their fluid inclusions associated with the Athabasca Basin ore bodies (Pagel et al. 1980; Hoeve et al. 1986; Wilson and Kyser, 1987; Kotzer and Kyser 1995), no Sr and Nd isotopic and trace element data have been reported for dolomite veins.

Along the brine flow path, brine-rock interactions have been key events in the mineralizing process because: (i) brine-rock interactions are at the origin of the chemical evolution of evaporated seawater into two chemically distinct NaCl-rich and $CaCl_2$-rich brines, whose mixing is coeval with $UO_2$ deposition (Derome et al., 2005; Richard et al., 2010); (ii) basin and basement rocks contain various potential U sources (Fayek and Kyser, 1997; Hecht and Cuney, 2000; Mercadier et al., 2013) and (iii) basement rocks host potential U-reducing agents, necessary for the reduction of U(VI) to U(IV) and $UO_2$ deposition (Hoeve and Quirt, 1987).

Many aspects of the evolution of brines through brine-rock interaction and U mineralization remain contentious and are addressed in this paper: (i) the degree of isotopic (and chemical) equilibration between the brines and host rocks (Pagel et al., 1980; Wilson and Kyser, 1987; Kotzer and Kyser, 1995); (ii) the magnitude of temperature variation during the ore-forming events (e.g. Alexandre et al., 2005; Derome et al., 2005); (iii) the mobility of REE which can substitute for up to ~1 wt.% of the U in $UO_2$ (Fayek and Kyser, 1997; Mercadier et al., 2011a) and whose content is in the order of tens to hundreds of ppm La and Ce in the fluid inclusions (Richard et al., 2013); (iv) the nature of gases produced by interaction between brines and graphitic metapelites in the basement (e.g. Bray et al., 1988; Kyser et al., 1989) and (v) the origin of anomalously-low δD values of alteration minerals around U-ores (e.g. Kotzer and Kyser, 1991; Halter et al., 1987).

111 ## 2. GEOLOGY, SAMPLING AND FLUID INCLUSIONS

112

113 ### 2.1. Regional geology

114

115 The Athabasca Basin unconformably overlies the Archean to Paleoproterozoic
116 Western Churchill Province separated into two Subprovinces (the Rae Subprovince in the
117 west and the Hearne Subprovince in the east) by the Northeast-trending Snowbird tectonic
118 zone (Hoffman, 1990; Card et al., 2007; Jefferson et al., 2007) (Fig. 1A). These two
119 subprovinces consist of Archean gneisses, Paleoproterozoic metapelites and mafic to felsic
120 intrusions. They were affected respectively by the ~2.0 to ~1.9 Ga Thelon-Talston and the
121 ~1.9 to ~1.8 Ga Trans-Hudson orogenies (Chiarenzelli et al., 1998; Annesley et al., 2005). A
122 majority of the known unconformity-related U deposits of the Athabasca Basin, are located
123 close the transition between two lithostructural domains of the Hearne Subprovince, known as
124 the Wollaston-Mudjatik transition zone that consists of a Northeast-trending, anastomosing
125 structure of Hudsonian age (1.8 Ga) (Annesley et al., 2005).

126 The sedimentary sequence of the Athabasca Basin (the Athabasca Group), was
127 deposited starting from ~1.75 Ga (Ramaekers et al., 2007). The current maximum thickness of
128 the sedimentary cover is ~1.5 km and could have reached ~5 km based on P-T estimations
129 from fluid inclusions (Pagel, 1975; Derome et al., 2005). From the base to the top, the
130 Athabasca Group is composed of fluvial to marginal marine quartz-rich sandstones (Fair
131 Point, Read, Smart and Manitou Falls Formations), marine sandstones, phosphatic siltstones,
132 and phosphatic mudstones (Lazenby Lake and Wolverine Point Formations), fluviatile
133 sandstones (Locker Lake and Otherside Formations), shales (Douglas Formation) and finally
134 stromatolitic carbonates (Carswell Formation) (Ramaekers et al., 2007). The Douglas and

Carswell formations are only preserved around the Carswell meteoritic structure (Pagel et al., 1985; Genest et al., 2010).

### 2.2. Unconformity-related U deposits

The unconformity-related U deposits are generally located near the basement/cover interface, and structurally controlled by sub-vertical faults rooted in graphite-rich basement metapelites. The spatial distribution of the ore and alteration minerals around the unconformity greatly vary between the deposits. The $UO_2$ ores can be basement-hosted (e.g. P-Patch, Eagle Point and Millennium), unconformity-hosted (e.g. McArthur River, Rabbit Lake) or sandstone-hosted (e.g. Cigar Lake) sometimes in the same deposit (e.g. Shea Creek).

The earliest $UO_2$ ores in the Athabasca Basin have been dated between 1.5 and 1.4 Ga and successive late episodes of mineralization and/or recrystallization occurred up to ~0.7 Ga (Cummings and Krstic, 1992; Fayek et al., 2002; Alexandre et al., 2009a; Alexandre et al., 2012). Remobilization of primary $UO_2$ by meteoric fluids likely occurred around 400 Ma and then up to recent times (Mercadier et al., 2011b).

The main alteration features associated with U ores include successively: (i) partial to complete replacement of the initial basement minerals (K-feldspar, biotite, plagioclase) by an illite + sudoite (Mg-chlorite) ± dravite (Mg-tourmaline) assemblage (also referred as "bleaching") as well as the precipitation of illite and sudoite in sandstones; (ii) quartz dissolution in basement rocks as well as in the sandstones; (iii) precipitation of dravite + quartz + $UO_2$ + dolomite + bitumen in quartz dissolution vugs and in veins and breccias (Derome et al., 2005; Mercadier, 2010). A simplified mineral paragenesis summarizing petrographical observations of U deposits throughout the Athabasca Basin is shown in Figure 1B. Quartz and dolomite veins are spatially associated with the main alteration minerals and

U mineralization (Fig. 1B; Pagel et al., 1980; Kotzer and Kyser, 1995; Kyser et al., 2000; Derome et al., 2005).

### 2.3. Sampling and samples

Six U deposits from the Athabasca Basin have been sampled for this study (McArthur River, Rabbit Lake, Shea Creek, P-Patch, Millennium and Eagle Point), covering various mineralized areas in the basin (Fig. 1A). These deposits share the typical characteristics of unconformity-related U deposits described above (Hoeve and Sibbald, 1978; Heine, 1986; Kotzer and Kyser, 1995; Lorilleux et al., 2002; Derome et al., 2005; Alexandre et al., 2005; Laverret et al., 2006, 2010; Le Carlier de Veslud et al., 2009; Cloutier et al., 2009, 2011; Mercadier et al., 2010, 2011b).

Sampling was mainly focused on basement-hosted vein systems, concistently with the aim to track brine-rock interaction, and also because of a lack of preserved sedimentary cover (i.e. Rabbit Lake and Eagle Point) and lack of sandstone-hosted veins (P-Patch and Millennium). Only four quartz veins were sampled in sandstones at Shea Creek (IF23, IF29, IF41, IF98) at 20 to 30 m above the unconformity. A total of 49 quartz veins and 20 dolomite veins were sampled, the depth of which below the unconformity ranged from 13 m (EPE44-17, Eagle Point) to 361 m (EPE44-14, Eagle Point; Table 1). The veins crosscut various lithologies such as gneisses, pegmatoids and sandstones, with varying degrees of alteration. Figure 2A-F shows some typical quartz and dolomite veins studied in this work. In veins containing both quartz and dolomite (Fig. 2C, D), dolomite growth post-dates quartz growth.

183 **2.4. Fluid inclusions**

184

185 In quartz and dolomite veins, mainly 5 to 25 µm two phase (liquid + vapor) and three
186 phase (liquid + vapor + halite) fluid inclusions are observed (Fig. 2G; Pagel et al. 1980;
187 Derome et al. 2005). The volumetric fraction of the vapor phase is between 5 and 15% with
188 maximum frequency around 10%. A minority of inclusions contain solids such as of hematite
189 and/or phyllosilicates, both interpreted as daughter minerals due to their relatively constant
190 volume compared to the volume of fluid inclusions. The fluid inclusions have negative crystal
191 or more irregular shapes and are found either along growth bands of the host mineral, as
192 clusters of fluid inclusions, or as isolated inclusions. Therefore, the petrographic evidence
193 suggests that the brine inclusions are either primary or pseudosecondary and coeval with the
194 formation of their host minerals. Very minor amounts of low-salinity inclusions similar to
195 those described in Derome et al. (2005) are present along secondary fluid inclusion planes
196 indicative of healed microfractures.

197 Detailed microthermometric analysis and P-T reconstruction of quartz-hosted fluid
198 inclusions from McArthur River revealed that the brines at the time of origin of quartz veins
199 formation circulated at temperatures of ~110-220°C (Derome et al. 2005). Analyses of fluid
200 inclusions hosted in quartz veins associated with the U ores (microthermometry, laser-induced
201 breakdown spectroscopy (LIBS) and laser ablation-inductively coupled-mass spectrometry
202 (LA-ICP-MS)) have enabled reconstruction of the chemical composition of the U-
203 mineralizing brines. A continuum of compositions between a Cl-Na-Ca-Mg-K brine end-
204 member ("NaCl-rich brine") and a Cl-Ca-Mg-Na-K end-member ("$CaCl_2$-rich brine") has
205 been interpreted as the result of mixing between the two end-members at the time of U
206 deposition (Derome et al., 2005; Richard et al., 2010). The two brines have a salinity of 25-35
207 wt.% salts and have carried U in concentrations up to ~600 ppm (Richard et al., 2010; 2012).

Synchrotron analyses of U-bearing fluid inclusions have shown that the U remains in the U(VI) form (the most soluble from) at room temperature and up to homogenization temperature (150-200°C) (Richard et al., 2013).

Here, the fluid inclusions in the studied samples (quartz and dolomite veins) share all the petrographic characteristics typical of those found in the Athabasca deposits. Detailed microthermometric data for the studied samples will be presented in a separate publication (Richard et al., submitted). Briefly, microthermometric observations have shown that the samples analyzed here contain variable amounts of the NaCl-rich brine and $CaCl_2$-rich brine. Homogenization temperatures in quartz- and dolomite-hosted fluid inclusions are predominantly 80 and 150°C, and comparable to those found at McArthur River (Derome et al., 2005). However, their interpretation in term of trapping temperature in subjected to assumptions on: (i) the pressure regime (hydrostatic vs. lithostatic), (ii) possible post-trapping deformation and (iii) possible influence of radiolytic gases ($H_2$, $O_2$). This results in large uncertainty on the actual P-T conditions of the brines at the time of trapping and it has been proposed that the temperature of the brines was between 110 and 220ºC (Derome et al. 2005; Richard et al., submitted).

## 3. ANALYTICAL METHODS

### 3.1. Analysis of quartz and dolomite veins

The analysis of major and trace elements in dolomite samples was performed on dolomite separates obtained by hand picking under the binocular microscope. Fine powders were obtained by crushing in an agate mortar. Powders were analysed at the SARM laboratory (CRPG-CNRS, Nancy, France). Chemical compositions of dolomite powders (300

mg) were obtained, after $LiBO_2$ fusion and dissolution by $HNO_3$, by inductively coupled plasma-optical emission spectroscopy (ICP-OES) for major elements and inductively coupled plasma-mass spectrometry (ICP-MS) for trace elements (Table 2) following the method of Carignan et al. (2001). Detection limits and analytical uncertainties are given in Table 2.

The oxygen isotope composition of quartz was analyzed at the stable isotope laboratory of Géosciences (University of Rennes 1, France). Pure quartz grains were separated by handpicking under a binocular microscope and ground in a boron carbide mortar. In order to remove $O_2$ from quartz, about 6-7 mg of quartz powder were reacted overnight with BrF5 at 670°C using the methodology of Clayton and Mayeda (1963). $O_2$ was then converted into $CO_2$ by reaction with hot graphite. $CO_2$ was analyzed isotopically using a VG SIRA 10 triple collector mass spectrometer. Values of $\delta^{18}O$ for quartz are reported in standard per mil (‰) notation relative to V-SMOW (Vienna Standard Mean Ocean Water). Analyses were performed on distinct analytical sessions involving two bottles of $BrF_5$ reagent and the measured $\delta^{18}O$ values were slightly corrected given the specific value obtained on the NBS28 international standard and the in-house A1113 granite standard for each session; the amplitude of $\delta^{18}O$ correction was between +0.19 and +0.46‰. Taking into account standard correction and internal reproducibility, the analytical uncertainty for quartz $\delta^{18}O$ values is ±0.2‰ (1σ).

The oxygen and carbon isotope composition of dolomite were analyzed at the stable isotope laboratory of Géosciences (University of Rennes 1, France). Pure dolomite grains were separated by handpicking under the binocular microscope and ground in a boron carbide mortar. $CO_2$ was extracted from about 10 mg of carbonate powders by reaction with anhydrous phosphoric acid ($H_3PO_4$) in vessels at 50°C for 12 hours using the methodology of McCrea (1950). $CO_2$ was then analyzed isotopically using a VG SIRA 10 triple collector mass spectrometer. Values of $\delta^{13}C$ for dolomites are reported in standard per mil (‰) notation

relative to V-PDB (Vienna Pee Dee Belemnite). The oxygen isotope composition of dolomites (relative to V-SMOW) was calculated assuming pure dolomitic composition and experimental fractionation coefficients $\alpha_{Dol-CO2}$ = 1.01065 at 50°C (Rosenbaum and Sheppard, 1986). During the analytical session, measurements on Prolabo Rennes in-house standard and NBS 19 limestone international standard were used to correct the measured $\delta^{18}O$ and $\delta^{13}C$ values by less than 0.1‰. Taking into account standard correction and internal reproducibility, the analytical uncertainty is better than ±0.1‰ for $\delta^{13}C$ (1σ) and about ±0.1‰ for $\delta^{18}O$ (1σ).

Sr isotope analyses on dolomite samples were carried out at the geochemical laboratory of Géosciences (University of Rennes 1, France). About 10 mg of each powdered sample were dissolved in 2N cold HCl for one hour. Solutions were then centrifuged, dried and redissolved 2N cold HCl for Sr separation using standard chromatographic column cation separation (BioRad AG 50WX8 resin, H+ form, 200-400 mesh). Total blank was 100 pg and was considered as being negligible. Sr was analyzed isotopically using a Finnigan Mat 252 multi-collector mass spectrometer. During the two analytical sessions, repeated measurements on NBS 987 gave a mean $^{87}Sr/^{86}Sr$ ratio of 0.710195 (2σ, N=5) and the measured $^{87}Sr/^{86}Sr$ ratios were adjusted to the standard value of 0.710250±7.

Nd isotope analysis of dolomite samples were performed at the SARM laboratory (CRPG-CNRS, Nancy, France). 100 to 200 mg of powdered samples were digested in screw-top Savillex® Teflon vials using a 4 ml $HNO_3$ (sub-boiled, 14M) and 1 ml HF (ultrapur Seastar, 28M) mixture on a hot plate (115°C) for 24-48h and then slowly evaporated. Subsequently, 4 to 5 ml of concentrated (sub-boiled, 11M) HCl was added to minimize fluoride formation and the solution was dried again. 2 ml of 2M $HNO_3$ were added before Nd separation. Nd was separated and purified using conventional anion exchange methods on columns containing Tru Spec and Ln Spec resins (Pin et al., 1994; Pin and Santos Zalduegi,

1997). Nd isotope compositions were measured on a Micromass Isoprobe multi collector-inductively coupled plasma-mass spectrometer (MC-ICP-MS). Mass fractionation was corrected using an exponential law and $^{146}Nd/^{144}Nd$ ratios = 0.72190 as the normalization ratio (Luais et al., 1997). Repeated analysis of an in-house JMC Nd standard yielded a $^{143}Nd/^{144}Nd$ value of 0.512241±32 (2σ, N=10) during the analytical session. Procedural blanks were negligible with values below 100 pg.

### 3.2. Analysis of fluid inclusions

The analysis of hydrogen and carbon isotope compositions of bulk fluid inclusions populations in quartz and dolomite was carried out at the CRPG-CNRS laboratory, Nancy, France. Quartz and dolomite veins were crushed to a grain size of 1-5 mm and separated by handpicking under the binocular microscope to avoid mineral impurities. Quartz and dolomite grains were then heated at 100°C overnight to remove atmospheric water before analyses. 2-8 g of quartz or dolomite grains were crushed in stainless steel tubes under vacuum at 110°C. Liberated $H_2O$ and $CO_2$ were collected in a liquid nitrogen cold trap and non-condensable volatiles (e.g. $H_2$, $O_2$, $CH_4$, and $N_2$) were evacuated. This methodology prevents from contamination of $H_2O$ and $CO_2$ by possible solid bitumen in the dolomite lattice. In order to separate $CO_2$ from $H_2O$, the liquid nitrogen trap was replaced by an alcohol + liquid nitrogen slush trap at -80°C. The liberated $CO_2$ was trapped in a liquid nitrogen cold trap and the amount of recovered $CO_2$ was measured in a calibrated volume using a Keller manometer. Then, $CO_2$ was extracted and analyzed isotopically using a VG Micromass 602D mass spectrometer. Values of $\delta^{13}C$ for $CO_2$ are reported in standard per mil (‰) notation relative to V-PDB. Only dolomite grains contained sufficient quantities of $CO_2$ to be analyzed isotopically. Standard $CO_2$ samples reproduced to within ± 0.1‰ (2σ). Owing to the small

amounts of recovered $CO_2$ (typically 1 µmole, molar $H_2O/CO_2$ = 30 to 400), $\delta^{13}C$ values are given with a rather large uncertainty of ± 5‰. Water was liberated from the -80°C trap and passed through a U furnace at 800°C where $H_2O$ was reduced to $H_2$. $H_2$ was then pumped using a Toepler pump. The recovery of $H_2$ from $H_2O$ is assumed to be of 100%. The amount of $H_2$ was measured in a calibrated volume using a Keller manometer. Then $H_2$ was extracted and analyzed isotopically using a VG Micromass 602D mass spectrometer. Values of δD for $H_2$ and thus for fluid inclusions $H_2O$ are reported in standard per mil (‰) notation relative to V-SMOW. When introduced into the same vacuum line with a vacuum-tight micro-syringe, ED3 standard (-60‰) reproduced to within ±2‰ (2σ).

## 4. RESULTS

### 4.1. Stable isotope (O, C) composition of quartz and dolomite veins

Stable isotope data for quartz and dolomite veins are shown in Table 1 and Figure 3. They are broadly consistent with those published by Pagel et al. (1980), Hoeve et al. (1986), Wilson and Kyser (1987) and Kotzer and Kyser 1995) for Rabbit Lake, McArthur River and Key Lake deposits.

The $\delta^{18}O$ values of quartz range between 11.9 and 17.4‰, with 41 values on 49 lying between 14 and 17‰. The highest values are recorded at Millennium and Eagle Point ($\delta^{18}O$ = 15.3 to 17.4‰), intermediate values at P-Patch, Shea Creek and Rabbit Lake ($\delta^{18}O$ = 12.9 to 16.9‰), and the lowest values at McArthur River ($\delta^{18}O$ = 11.9 to 16.0‰). The $\delta^{18}O$ values of dolomite range from 13.1 to 23.8‰ with no clear difference between deposits. Nearly all quartz-dolomite pairs (MAC5, P48-3, RBL14, RLB2, RLB5 and RLB7; Table 1) show isotopic reversal with the $\delta^{18}O$ value of dolomite being higher than the quartz value (RLB5 is

an exception). Also, in Figure 3A, the dolomite histogram is displaced to the right when compared to the quartz one, which shows that the isotopic disequilibrium between dolomite and quartz is the rule rather than the exception in the Athabasca Basin ore deposits. There is no clear relationship between the $\delta^{18}O$ value of quartz and dolomite and their sampling depth below unconformity (Table 1).

The $\delta^{13}C$ values of dolomite range from -23.5 to -3.5‰ with a majority of values between -3.5 and -8‰. There is no significant difference between deposits, and the extremely low value of -23.5‰ measured in only one sample from the McArthur River deposit can hardly be considered as representative of the whole site. No correlation is observed between the $\delta^{13}C$ and $\delta^{18}O$ values of dolomite (Fig. 3C).

**4.2. Stable isotope (H, C) composition of fluid inclusions**

Hydrogen and carbon isotope data for quartz- and dolomite-hosted fluid inclusions are shown in Table 1 and Figure 3B,C. The heterogeneity of samples was tested by analyzing two or three separates of individual veins. Replicate analyses show that some samples have quite reproducible δD values (±2‰) while other samples display larger variability (±10‰), as noted by Pagel et al. (1980) for comparable measurements on Rabbit Lake samples. The δD values reported in Table 1 correspond to the average value among two or three replicate analyses. Therefore, a conservative uncertainty of ±10‰ was applied to all δD values. This high internal variability is well beyond analytical reproducibility (±2‰; 2σ) and is attributable to heterogeneities at the scale of individual veins. A minor influence of phyllosilicate daughter phases in fluid inclusions cannot be ruled out. Heterogeneities at the scale of individual veins may also account for the variability of the $\delta^{13}C$ values which are given with a conservative uncertainty of ±5‰.

358 The δD values of quartz-hosted fluid inclusions range from -52 to -110‰
359 (predominantly above -70‰). The δD values of dolomite-hosted fluid inclusions range from -
360 46 to -147‰ (predominantly above -70‰). The new data presented here compare broadly to
361 the few published data from Pagel et al. (1980) and Kotzer and Kyser (1995) for Rabbit Lake
362 dolomite and McArthur River quartz respectively (Fig. 3B). For Eagle Point and Rabbit Lake
363 deposits, the δD values of dolomite-hosted fluid inclusions are higher than for quartz-hosted
364 fluid inclusions. The reverse relationship is observed for McArthur River deposit. At P-Patch
365 δD values of dolomite-hosted and quartz-hosted fluid inclusions overlap. Combined with the
366 fact that the number of data is rather small for each deposit, it can be concluded that there is
367 no general rule for discrimination of δD values between dolomite-hosted and quartz-hosted
368 fluid inclusions. In veins where both quartz and dolomite precipitated, the δD values of
369 quartz-hosted and dolomite hosted fluid inclusions differ significantly. Generally, the δD
370 value of quartz-hosted inclusions is below that of dolomite-hosted inclusions, the two
371 exceptions being samples P48-3 and MAC5. The δD values of fluid inclusions and the $\delta^{13}C$
372 values of $CO_2$ do not show any relationship to depth below unconformity. No $CO_2$ was
373 recovered from quartz veins whereas small amounts of $CO_2$ were recovered from dolomite
374 veins (see Section 3.2.). This explains why, in spite of their differences in their $CO_2$ content,
375 no $CO_2$ was detected in dolomite-hosted fluid inclusions during microthermometry and
376 quartz- and dolomite-hosted fluid inclusions show similar microthermometric characteristics.
377 The $\delta^{13}C$ values of $CO_2$ dissolved in dolomite-hosted fluid inclusions are mostly between -8
378 and -19‰ with two noticeable exceptions at -4‰ (sample RBL14) and -30‰ (sample
379 MAC5). Interestingly, the lowest $\delta^{13}C$ values of $CO_2$ and dolomite, corresponds to the lowest
380 δD value (sample MAC5).
381

### 4.3. Chemical composition of dolomite veins

Chemical compositions are reported in Table 2. The Mg/Ca molar ratio is most often close to unity and indicates pure dolomite, except in Eagle Point and McArthur River samples where a minor ankeritic component is present. Also, some samples contain a significant amount of quartz (samples P55-15, RLB2 and RLB9), with an associated dilution of trace element contents hosted in dolomite (Sr). The U content of dolomite veins is up to 16 ppm in sample MAC5 and 152 ppm in sample P48-3, possibly due to tiny U-bearing mineral inclusions. Interestingly, these two samples have also the lowest δD values of fluid inclusions. The Sr content is between 16 and 60 ppm, which corresponds to classical contents for dolomites. The Rb content is consistently very low, generally below the detection limit (bld) (maximum = 1.96 ppm, sample H1935-8). Some elements show variable content, for example Cu between bdl and more than 300 ppm (sample RBL2). Noteworthy P-Patch samples are enriched in As (between 2 and 8 ppm). Variable Cu and As contents are possibly attributable to sulphide mineral inclusions.

Figure 4 shows the PAAS-normalized REE spectra of dolomite. The REE patterns of dolomite samples are homogeneous, with LREE depleted patterns, a generally upward convex pattern and flat HREE pattern close to the PAAS abundance. Three samples display relatively flat REE patterns and positive Eu anomaly. The first group of dolomite displays a tetrad effect pattern. Sample MAC5 has very low REE content below the detection limit for most REE (Table 2; not shown in Figure 4).

### 4.4. Radiogenic isotope (Sr, Nd) composition of dolomite veins

The Sr isotope composition of dolomite (Table 3) is rather homogeneous between 0.705 and 0.711, with sample H1935-8 displaying a more radiogenic composition of 0.718. $^{87}Sr/^{86}Sr$ initial ratios were calculated at t = 1250 ± 250 Ma, which covers the most probable ages of U mobilization and precipitation of dolomite in the Athabasca system (Cummings and Krstic, 1992; Fayek et al., 2002; Alexandre et al., 2009a). These Sr initial isotope ratios are not very different from present-day ratios because of the very low Rb content of dolomite. At 1250 ± 250 Ma, the Nd isotope composition of dolomite varies much more than the Sr isotope ratios as the $\varepsilon_{Nd}(t)$ value is between -8.8 and -20.3. The data from the three studied deposits plot in distinct fields (Fig. 5) and $^{87}Sr/^{86}Sr_i$ and $\varepsilon_{Nd}(t)$ values show no clear relationship with each other or with another isotopic system, for a given deposit. Removing sample H1935-8 from the whole database, it is however possible to identify a negative correlation between the two isotopic compositions.

## 5. DISCUSSION

### 5.1. Quartz-dolomite veins in the mineralizing process

#### *5.1.1. Quartz-dolomite isotopic disequilibrium and temperature variation*

Microthermometric data on fluid inclusions do not provide better estimate than the range 110-220°C for the temperature of quartz and dolomite precipitation (see Section 2.4.). Also, chemical data on quartz- and dolomite-hosted fluid inclusions indicate that both minerals equilibrated with comparable brines.

Figure 3A shows the theoretical $\delta^{18}O$ value of dolomite in isotopic equilibrium at 180°C (as a working hypothesis) with the quartz veins. The dolomite with $\delta^{18}O > 19‰$ could not be equilibrated with the quartz veins, as also shown in veins where both quartz and dolomite precipitate (see Section 4.1.). Instead, the high $\delta^{18}O$ value of dolomite indicates mineral precipitation at lower temperature or from a higher $\delta^{18}O$ fluid (or a combination of both). Two arguments plead for a temperature decrease. First, a lower temperature event is consistent with paragenetic observations because dolomite crystals generally formed later than quartz in veins (Fig. 2C, D) and thus at lower temperature in a cooling system. Second, the brine from which dolomite formed resembles the one from which quartz did, which implies that on a first order, the $\delta^{18}O$ value of the fluid was comparable in both cases and that only a temperature decrease for the dolomite stage can explain the high $\delta^{18}O$ value of this mineral. As a crude estimate, the isotopic difference between quartz and part of the dolomite ($\delta^{18}O > 19‰$) may indicate a temperature of precipitation decrease of ~ 50-100°C within the 110-220°C range defined by fluid inclusion microthermometry.

Consistently, when considering the uncertainty on $\delta^{13}C$ values of $CO_2$, most $\delta^{13}C_{CO2}$ - $\delta^{13}C_{Dol}$ pairs indicate apparent temperature of dolomite crystallization (and fluid inclusion trapping) ranging between 50 and 150°C (Ohmoto and Rye, 1979). Although this is a crude estimate, this is consistent with the idea that dolomite precipitation documents a lower temperature event than the quartz stage.

Dolomite precipitation during cooling is at variance with the theoretical increase of dolomite solubility with cooling (Bertram et al., 1991; Burton and Walter, 1991; Warren 2000; Lopez et al., 2009). Cooling was not responsible by itself for dolomite precipitation. Precipitation of hydrothermal dolomite from Na-Ca-Mg brines at comparable temperatures is well documented in sedimentary environments (e.g. Gleeson and Turner 2007 ; Conliffe et al. 2010 ; Gormek et al., 2012). Dolomite precipitation is partially controlled by the Ca/Mg

454 content of the fluids. Here, microthermometrically similar fluid inclusions do not suggest
455 drastic change in Ca/Mg during the quartz and the dolomite stages. Subtle changes in Ca/Mg
456 would however be difficult to identify by microthermometry only due to comparable phase
457 relationships between the $H_2O$-NaCl-$CaCl_2$ and $H_2O$-NaCl-$MgCl_2$ systems (Dubois and
458 Marignac 1997 ; Steele McInnis 2011). In addition, Mg and Ca in dolomite-hosted fluid
459 inclusions cannot be determined by LA-ICP-MS due the high Ca and Mg content of the host
460 mineral. An independent factor of dolomite precipitation is thus necessary and might be found
461 in the increase in partial pressure of ($pCO_2$) in the fluid phase, which is documented by the
462 recovery of $CO_2$ in dolomite-hosted fluid inclusions.
463
464 *5.1.2. Isotopic equilibrium between quartz and alteration minerals*
465
466 Figure 3A shows a compilation of the published $\delta^{18}O$ values of the main alteration
467 minerals paragenetically associated with U ores throughout the Athabasca Basin (illite,
468 chlorite and dravite). Only the $\delta^{18}O$ values of pure illite, chlorite and dravite separates have
469 been considered here; they have been compiled from the following sources: Pagel et al.
470 (1980); Hoeve et al. (1986); Halter et al. (1987); Wilson et al. (1987); Bray et al. (1988);
471 Kotzer and Kyser (1991); Percival et al. (1993); Kotzer and Kyser (1995); Alexandre et al.
472 (2005, 2009b) and Cloutier et al. (2009, 2010, 2011). The $\delta^{18}O$ values of chlorite are highly
473 variable (2-18‰) but with very few values above 12‰. The $\delta^{18}O$ values of illite and dravite
474 range from 8 to 13‰. The theoretical range of $\delta^{18}O$ values of quartz in isotopic equilibrium
475 with the alteration minerals at 180°C was calculated using the fractionation factors of Wenner
476 and Taylor (1971), Eslinger and Savin (1973), Kotzer et al. (1993) and Zheng (1993a, b).
477 Several issues arise from this data compilation. The spread of $\delta^{18}O$ values of alteration
478 minerals goes well beyond simple temperature variation effects if the $\delta^{18}O$ of the fluid

remains nearly constant. The $\delta^{18}O$ values of quartz show a pronounced skew to low values that would indicate unreasonably high temperature if quartz was isotopically equilibrated with alteration minerals. Further work is needed on carefully selected alteration mineral + quartz assemblages to solve these problems. In spite of these uncertainties, the isotopic composition of quartz veins analyzed here compares rather well with the calculated isotopic composition of quartz at isotopic equilibrium with alteration minerals at 180°C (Fig. 3A). This calculation shows that quartz veins and alteration minerals are in global isotopic equilibrium near 180°C and therefore likely belong to a single event of alteration.

*5.1.3. Genetic link between dolomite and $UO_2$*

Besides $UO_2$, the main REE-bearing minerals in the vicinity of the studied deposits are monazite and zircon. During hydrothermal alteration, Hecht and Cuney (2000), Fayek and Kyser (1997), Gaboreau et al. (2007) and Mercadier et al. (2011a) have proposed that the REE were redistributed from monazite and zircon to aluminum phosphate-sulfate minerals (APS) and $UO_2$. In Figure 4 the REE spectra of dolomite are clearly distinct from those of typical seawater, monazite, zircon and APS (florencite). The REE upward convex patterns with tetrad effects are comparable in shape to those of $UO_2$ grains from the McArthur River deposit (Mercadier et al., 2011a), the main if not the only difference being the enrichment in MREE and HREE. In the $UO_2$, the major enrichment compared to PAAS is centered on Dy, the element most readily incorporated in the $UO_2$ crystal structure. Thus, it has been inferred that the REE patterns reflect differences in partition coefficients between $UO_2$ and a single fluid phase (Mercadier et al., 2011a). Here, major enrichment centered on Dy is also observed in dolomite and cannot be related to possible tiny $UO_2$ inclusions in dolomite lattice because the U and REE contents of dolomite are not correlated (Table 1). By consequence, some

504 particularities of the REE patterns may be partly representative of the fluid itself (i.e. LREE
505 depletion, tetrad effect, enrichment centered on Dy and flat HREE patterns). These results
506 highlight that dolomite and $UO_2$ incorporated REE from a similar source, even if $UO_2$ slightly
507 predated dolomite precipitation in the paragenetic sequence. This idea is consistent with the
508 comparable Nd isotope signature of the two minerals ($\varepsilon_{Nd}(t)$ between -10 and -25). The very
509 low REE content in sample MAC5 (not shown in Figure 4) could be related to massive
510 incorporation of REE within $UO_2$, a process that would be specific to the very high-grade,
511 large tonnage McArthur River deposit.

512 In Figure 5, the overall negative correlation visible excluding the high $^{87}Sr/^{86}Sr$ sample
513 (sample H1935-8 from Eagle Point) can be classically interpreted as a mixing hyperbola
514 involving at least two sources, one encountered in the Archean basement, the other one being
515 Proterozoic seawater (from which the mineralizing brines ultimately originate). In this
516 context, the large variation in $\varepsilon_{Nd}(t)$ value in most dolomite veins when compared to the
517 variation of the $^{87}Sr/^{86}Sr$ ratio may be related to the higher Sr content of brines. Indeed, when
518 brines interact with basement rocks, they are more able to keep their original Sr signature
519 rather than their Nd one given that $(Sr/Nd)_{brine} >> (Sr/Nd)_{basement}$. The $UO_2$ data locate at the
520 lower right side of the dolomite field and have isotopic compositions closer to host basement
521 rocks (Archean basement and local gneiss). It seems then that the brines at the origin of the
522 $UO_2$ stage interacted to some more extent with basement rocks than the one related to the
523 dolomite stage.

524 Sample H1935-8 has a peculiar position with regard to the whole dolomite population,
525 but it clearly points to a major contribution of the local gneiss in its Sr isotope composition, as
526 does the other sample from Eagle Point (ES-287-1) to a lesser extent. Also, the fact that the
527 dolomite population of each deposit has distinct Sr and Nd isotope compositions likely
528 indicates that each population records distinct fluid-rock interactions characteristics, in terms

of fluid/rock ratios and possibly the nature of the rock with which brines interacted (i.e. local heterogeneities in the basement). Qualitatively, this could possibly indicate that the dolomite stage resulted from small (or local) scale fluid movement, whereas the $UO_2$ stage may have resulted from some larger (or regional) scale fluid movement. Such a decrease of scale of fluid circulation is consistent with the lowering of the temperature between the quartz precipitation stage (synchronous with $UO_2$ precipitation) and the dolomite stage.

### 5.2. Evolution of brines through alteration and mineralization

#### *5.2.1. Reconstruction of the O isotope composition of brines*

Calculating the $\delta^{18}O$ values of brines is possible only if the precipitation temperature of quartz and dolomite is known. Here, microtherometric data indicate temperatures of 110-220°C (Derome et al. 2005; Richard et al., submitted) and oxygen isotope data indicate 50-100°C of temperature difference for crystallization between quartz and part of dolomite veins ($\delta^{18}O$ > 19‰; See Section 5.1.1.). Quartz and alteration minerals are isotopically equilibrated at around 180ºC (Fig. 3A; see Section 5.1.2.). Hence, a reasonable working hypothesis is that the dolomites with $\delta^{18}O$ > 19‰ have precipitated at temperature possibly around 120°C while dolomites with $\delta^{18}O$ < 19‰ have precipitated at higher temperatures, possibly up to 180°C. At these temperatures, the fractionation factors of Zheng (1993a) and Zheng (1999) are used to calculate the $\delta^{18}O$ value of fluids in equilibrium with quartz and dolomite by correcting minerals $\delta^{18}O$ value by -13.0‰ for quartz, -11.2‰ for dolomite precipitating at 180°C and -16.1‰ for dolomite precipitating at 120°C. A bulk uncertainty, taking into account analytical precision and an uncertainty of ± 30°C for temperature, is estimated at ± 2.5‰ for the $\delta^{18}O$ values of brines. Also, the effect of dissolved salts on mineral-$H_2O$ fractionation (the so-

called 'salt-effect') was estimated according to the regression of experimental data summarized in Chacko et al. (2003). This effect is dependent on the temperature of mineral precipitation, and amount of each dissolved major salts (NaCl, KCl, $CaCl_2$, $MgCl_2$). Using the amount of major salts from Richard et al. (2010), the isotopic data should be corrected by +0.4‰ and +1.1‰ for the veins that precipitated from a NaCl-rich brine and a $CaCl_2$-rich brine, respectively. Because most samples have precipitated in the presence of mixtures the two brines, an average salt correction of +0.7‰ was applied to all samples. The reconstructed $\delta^{18}O$ values of the mineralizing brines are reported in Figure 6, together with the δD measurement on fluid inclusions.

*5.2.2. Evidence for O, H isotope modifications*

In Figure 6, the position of present-day seawater and meteoric water line is reported for reference, as it is for other publications dealing with O and H isotope compositions in the Athabasca context (e.g. Wilson et al., 1987 ; Kotzer and Kyser, 1995), regardless of the debate as to whether such values are appropriate for the geological past (Lécuyer et al., 1996; Jaffrés et al., 2007; Pope et al., 2012). Displacing seawater composition within the possible range of its inferred past variations would induce a displacement of the star symbol figuring the parent brine from which the mineralizing brines evolved, but would not affect the body of evidence for O, H isotopic modifications as well as the internal variation of the present dataset. This isotopic dispersion is discussed below.

In the present dataset $\delta^{18}O$ - δD pairs are not available for all samples. There is no clear difference between deposits. The reconstructed compositions compare rather well with the few compositions available using the same methodology from McArthur River quartz (Kotzer and Kyser, 1995) and Rabbit Lake dolomite (Pagel et al. 1980) (Fig. 6). As already

depicted in the result section, it is apparent that some dolomite-hosted brines yield higher δD values than the corresponding quartz (see Rabbit Lake deposit for example). Many factors can account for the (O, H) composition of the brines.

Cl/Br ratios and stable chlorine isotope compositions have shown the NaCl and $CaCl_2$-rich brines originate from a common 'parent brine' derived from seawater evaporation beyond halite saturation (Derome et al., 2007; Richard et al., 2011; Leisen et al., 2012). In order to compare the composition of the brines from which quartz-dolomite veins have precipitated with the evaporated seawater from which they originate, the seawater evaporation trend was plotted in Figure 6 (Holser, 1979, Knauth and Beeunas, 1986). Assuming that seawater was evaporated up to epsomite saturation the residual brine would have $\delta^{18}O$ and δD values of ~ -3‰ and ~ -40‰ respectively.

As a whole, the calculated brine compositions are located on the lower right side of the Global Meteoric Water Line, and are clearly distinct from the composition of the parent brine (Fig. 6). Compared to the parent brine, $\delta^{18}O$ and δD values have been shifted by +2‰ to +10‰ and -5‰ to -100‰ respectively. Note that even though the exact temperatures of precipitation of quartz and dolomite are not precisely constrained by fluid inclusions (Derome et al., 2005), a positive $\delta^{18}O$ shift is found for the whole range of temperature invoked (110-220°C). Considering the uncertainties on the $\delta^{18}O$ value of the parent brine and on the temperature of quartz and dolomite precipitation, the magnitude of the positive shift (+2‰ to +10‰) should be considered as a guideline.

Although a positive $\delta^{18}O$ shift is expected in the context of intense fluid-rock interaction, one striking feature is the magnitude of δD shift compared to the parent brine. The δD values below -90‰ are comparable to those of organic water (i.e. water derived from reaction involving organic matter, Sheppard, 1986). Anomalously low δD fluids have been reported in a variety of geological environments (Gleeson et al. (1999) and references therein)

604 and a controversy has emerged on the significance of low δD values measured on bulk fluid
605 inclusion populations, alternatively interpreted as reflecting geological processes (e.g. mixing
606 with organic waters, membrane filtration, see Gleeson et al. (1999) for review), or
607 experimental artefacts (i.e. mixing between fluid inclusion water and structurally bound
608 water) (Simon, 2001; Gleeson et al., 2008). However, mechanical crushing at temperature
609 below 200°C appears to be a reliable method for δD analysis of bulk fluid inclusion
610 population (Simon, 2001) which supports that δD values presented here reflect the original δD
611 composition of the brines. In addition, during the experiments, there was no observed
612 relationship between the δD value and the amount of water liberated relative to the amount of
613 crushed mineral (typically 0.005 to 0.05 μmol/mg), meaning the potential contribution of
614 isotopically light structurally bound water is negligible.
615
616 *5.2.3. Origin of O isotope modifications*
617
618 One classical explanation for positive $\delta^{18}O$ shifts in hydrothermal waters is fluid-rock
619 interaction (Williams and McKibben, 1989). In the present work, positive $\delta^{18}O$ shifts between
620 evaporated seawater and the brines (+2 to +10‰, Fig. 6) could alternatively be caused by
621 diagenetic processes in the Athabasca Basin or fluid-rock interactions in the basement, under
622 low fluid/rock ratio conditions. By contrast, the intense alteration observed around
623 unconformity-related U deposits (see Section 2.2.) is more typical of high fluid-rock ratios
624 (Lorilleux et al., 2003).
625 Large variations in Na-Ca-Mg composition in the NaCl- and $CaCl_2$-rich brines
626 (Richard et al., 2010) can be attributed to either albitization of plagioclase or dolomitization
627 reactions (Davisson and Criss, 1996; Houston et al., 2011). Assuming a $\delta^{18}O$ value of 10‰
628 for plagioclase and initial $\delta^{18}O$ value of -3‰ for the evaporated seawater, significant positive

629 $\delta^{18}O$ shifts (> 2‰) due to albitization of plagioclase by evaporated seawater is only possible
630 at temperatures above 150°C and a $\delta^{18}O$ shift of +6‰ is only possible at 350°C (Zheng,
631 1993a) which is unreasonably high for the studied brines. Detrital plagioclase grains are
632 nearly absent from the preserved sedimentary succession (Ramaekers et al., 2007) and
633 albitization of basement plagioclase has not been observed (Mercadier et al., 2010). Hoeve
634 and Sibbald (1978) mentioned the occurrence of albite-rich plagioclasite at Rabbit Lake,
635 although their formation appears to be disconnected (anterior) to brine circulation. Therefore
636 even though albitization is a plausible cause for the high Ca/Na in the $CaCl_2$-rich brine, such a
637 reaction hardly accounts for most of the positive isotopic shift. Similarly, the widespread
638 illitization and chloritization of feldspar and biotite in basement rocks (Mercadier et al. 2010)
639 cannot be the unique cause for isotopic shift, considering that most of these alteration
640 minerals (illite, chlorite) have $\delta^{18}O$ values close to 10‰ (Fig. 3A). Assuming a $\delta^{18}O$ value of
641 30‰ for marine calcite and initial $\delta^{18}O$ value of -3‰ for the evaporated seawater,
642 dolomitization of calcite would readily produce residual fluids with $\delta^{18}O$ value up to 10‰
643 (Zheng, 1993a) in the range of temperature relevant to this study (25-200°C). Stromatolitic to
644 massive dolostones are described in the Carswell Formation (Ramaekers et al., 2007)
645 although the conditions for dolomitization have not been studied. Interaction with dolomitic
646 marbles in the basement (Annesley et al., 2005) is one possibility of acquiring heavy O
647 isotopic composition. Such a lithology has been recognised and has $\delta^{18}O$ values of 12-18‰ at
648 Rabbit Lake (Hoeve et al., 1986). Finally, mass balance considerations suggest that the
649 presence of some healed microfractures in quartz and dolomite (see Section 2.2.) could not
650 attest for significant modification of the primary O isotope composition of the host minerals.
651 Hence, further work is needed in order to specify the exact process responsible for the
652 positive $\delta^{18}O$ shift in the mineralizing brines. However, the results show that the mineralizing

653 brines have strongly re-equilibrated with host rocks at low fluid-rock ratios and distal to
654 alteration haloes.
655
656 *5.2.4. Origin of $CO_2$*
657
658 Alteration of graphite in basement metasediments is widespread in the vicinity of U
659 deposits of the Athabasca Basin and is spatially related to reactivated fault systems where
660 brine circulations were the most intense. This alteration results in partial to complete
661 dissolution and remobilization of graphite along faults (Kyser et al., 1989; Wang et al., 1989).
662 Hoeve and Sibbald (1978) proposed that $CH_4$ was the dominant product of brine graphite
663 interaction. Bray et al. (1988) proposed that interaction of brines with graphitic
664 metasediments could have produced $CO_2 \pm CH_4 \pm H_2S \pm H_2$ gases. They suggested that $CO_2$ was
665 the dominant product of graphite alteration based on gas chromatographic analysis of heated
666 illitic and chloritic material. Hoeve and Sibbald (1978) and Bray et al. (1988) both suggested
667 that the migration of gases (especially $CH_4$) produced by brine-graphite interaction was a
668 viable process for the reduction of U(VI) to U(IV) and subsequent $UO_2$ deposition. Based on
669 $\delta^{13}C$ measurements on unaltered and altered graphite, Kyser et al. (1989) concluded that $CO_2$
670 was also the dominant product of brine-graphite interaction, well beyond $CH_4$. Considering
671 $\delta^{13}C$ composition of graphite ranging from -30 to -20‰ (Kyser et al., 1989; Wallis et al.,
672 1986), and by using fractionation factors for graphite-$CO_2$ isotopic equilibrium (Ohmoto and
673 Rye, 1979), $CO_2$ in equilibrium with graphite resulting from brine-graphite interaction at 120-
674 180°C would have $\delta^{13}C$ values of ~ -15 to -5‰. Thus, the $\delta^{13}C$ values of dolomites and $CO_2$
675 dissolved in dolomite-hosted fluid inclusions are consistent with brine-graphite interaction at
676 120-180°C as the origin of $CO_2$ in the studied brines. In addition samples MAC5 and P48-3

677 display the lowest δD and $\delta^{13}C$ values of fluid inclusions in dolomites. This suggests a
678 possible link between C and H isotopic compositions.
679
680 *5.2.5. Origin of H isotope modifications*
681
682 The δD values of the main alteration minerals (illite, sudoite, dravite, kaolinite) have
683 been extensively studied in the Athabasca system (Wilson and Kyser, 1987; Bray et al., 1988;
684 Kotzer and Kyser, 1995; Alexandre et al., 2005; Alexandre et al., 2009b; Cloutier et al., 2009,
685 2010, 2011). In most works, the δD values were interpreted in terms of involvement of a
686 basin-derived fluid (δD = -40‰ to -70‰) and a basement-derived fluid (0‰ to -70‰). A
687 controversy has emerged from some extremely low δD values (δD < -70‰) which were
688 alternatively explained by: (1) primary equilibration with low δD fluids (Pagel et al., 1980;
689 Bray et al., 1988) ; (2) radiation-catalyzed hydrogen exchange (Halter et al., 1987) or (3) late
690 re-equilibration with meteoric waters (Wilson and Kyser, 1987; Wilson et al., 1987; Kyser
691 and Kerrich, 1990; Kotzer and Kyser, 1991, 1995; Alexandre et al., 2005; Alexandre et al.,
692 2009b). Up to now, the last hypothesis has prevailed.
693 The present results clearly show the presence of low δD brines. The unusually low δD
694 values of brines require the involvement of a low δD component. A good candidate for low
695 δD component is $H_2$ which was detected in variable amounts in fluid inclusions from
696 McArthur River deposits by Derome et al. (2003a, 2005) and mineralized areas from
697 Australian unconformity-related U deposits (Derome et al. 2003b). In these studies $H_2$ was
698 sometimes associated to $O_2$ within fluid inclusions and was interpreted as resulting from
699 water radiolysis. Water radiolysis is a common phenomenon in the environment of U deposits
700 (Dubessy et al., 1988; Savary and Pagel., 1997). $H_2$ produced by water radiolysis has δD of ~
701 -500‰ (Lin et al., 2005). According to Dubessy et al. (1988), water radiolysis could either

occur in any fluid in contact with U minerals, or within fluid inclusions having U-bearing daughter phase or dissolved U. Another possibility, compatible with statements from Dubessy et al. (1988), is that water radiolysis occurred within the mineralizing brines due to their high U content (Richard et al., 2010, 2012). In the latter case, dissolved and possibly molecular $H_2$ could have been present in the brines prior to the first stages of U deposition and could have acted as a reductant for U(VI).

Solid bitumens are widespread in the environment of unconformity-related U deposits (Landais and Dereppe, 1985; Leventhal et al., 1987; Landais et al., 1990, 1993; Landais, 1996 ; McCready et al., 1999 ; Alexandre and Kyser, 2006; McCready et al., 2007 ; Wilson et al., 2007). Petrographic analyses show that they formed during the late-ore stage. Based on $\delta^{13}C$ measurements on graphite and bitumen, Kyzer et al. (1989) concluded that graphite was a possible precursor for bitumen. Using ion microprobe $\delta^{13}C$ measurements on bitumen, Sangély et al. (2007) proposed that $CO_2$, originating from brine-graphite interaction, was combined with radiolytic $H_2$ to from hydrocarbons through Fischer-Tropsch-like reactions such as illustrated in the following equations:

$$n\text{-alkanes synthesis: } nCO_2 + (3n + 1)H_2 \rightarrow C_nH_{2n+2} + 2nH_2O$$

$$\text{naphtalene synthesis: } 10CO_2 + 24H_2 \rightarrow C_{10}H_8 + 20H_2O$$

Such reaction can produce low δD $H_2O$ from low δD $H_2$, although the δD value of $H_2O$ produced is difficult to estimate due to uncertainties in hydrogen isotopic fractionation between hydrocarbons and $H_2O$. If the δD value of water produced by these reactions is similar to that of radiolytic $H_2$ (~ -500‰), only a 10% mixing could account for a δD shift of brines from -50‰ to ~ -95‰. On the other hand, the residual water after radiolysis would acquire high δD values. This is hardly evidenced probably because radiolysis does not produce sufficiently high amount of low δD $H_2$, and associated high δD $H_2O$. This raises the question of mass balance consideration on the volume of low δD water produced by

727 combination of water radiolysis and Fisher-Tropsch-like reaction. Although this volume was
728 probably small, discrete and incomplete mixing between brines and low δD water could
729 account for not only for the low δD values of the mineralizing brines but also for (i) a minor
730 part of the observed variability in fluid inclusion salinity and (ii) the heterogeneity of
731 measured δD from one sample to another and even at the scale of individual quartz or
732 dolomite veins, as previously shown by Pagel et al. (1980).

733 Finally, the present results show that the low δD values of the mineralizing brines is
734 one possible explanation to the low δD values of alteration minerals. Late re-equilibration
735 with low temperature meteoric waters and radiation-catalyzed hydrogen exchange are not
736 incompatible with the involvement of low δD brines but their relative importance for
737 explaining low δD values of alteration minerals has to be re-evaluated.

738

739 **6. CONCLUSION**

740

741 The present study of quartz-dolomite veins and their fluid inclusions associated with
742 unconformity-related U ores documents the evolution of evaporated seawater towards U-
743 mineralizing brines.

744 Stable isotopes (O, H, C), radiogenic isotopes (Sr, Nd) and trace elements (including
745 REE) bring new insights into (i) the temperature variation during hydrothermal events
746 associated with high-grade alteration and $UO_2$ deposition, (ii) genetic links between quartz-
747 dolomite veins, alteration minerals (illite, chlorite and dravite) and $UO_2$, (iii) the extent of
748 equilibration between brines host rocks, (iv) the consequence of brine-graphite interaction in
749 the basement and water radiolysis for generating $CO_2$ and $H_2$ respectively, (iv) the implication
750 of Fisher-Tropsch-like reactions and abiogenic bitumen synthesis involving $CO_2$ and $H_2$ for

751 generating anomalously low δD brines, (v) the origin of the low δD values of alteration
752 minerals around U ores.

753 The main findings are that the alteration minerals, quartz-dolomite veins and $UO_2$
754 have been equilibrated with similar brines in a progressively cooling system (~180 to
755 ~120°C). The brine composition has been drastically shifted from the original one (evaporated
756 seawater) through extensive fluid-rock interactions, a key factor for efficient U mobilization
757 in the Athabasca system.

758

759 **ACKNOWLEDGEMENTS**

760

761 The authors thank CNRS and Areva NC for the financial support (BDI PhD grant for
762 A. Richard and J. Mercadier); Areva NC and Cameco for providing the samples and scientific
763 collaboration. The following colleagues are greatly acknowledged for their precious advice
764 and technical assistance during isotopic analyses: Christophe Cloquet (CRPG) for Nd isotopes
765 on dolomites; Caroline Guilmette, Maarten Lupker and Pierre Baillot (CRPG) for H, C
766 isotopes in fluid inclusions; David Vilbert and Krzysztof Surchorski (Univ. Rennes 1) for Sr
767 and O, C isotopes on dolomites respectively. The authors greatly appreciated insightful
768 comments by Anthony Fallick, Eric Potter and an anonymous reviewer, and editorial
769 suggestions by Ed Ripley.

770

771 **REFERENCES**

772

773 Alexandre P., Kyser K., Polito P. and Thomas D. (2005) Alteration mineralogy and stable
774 isotope geochemistry of Paleoproterozoic basement-hosted unconformity-type
775 uranium deposits in the Athabasca Basin, Canada. *Econ. Geol.* **100**, 1547–1563.

776 Alexandre P. and Kyser T. K. (2006) Geochemistry of uraniferous bitumen in the Southwest
777 Athabasca basin, Saskatchewan, Canada. *Econ. Geol.* **101**, 1605–1612.
778 Alexandre P., Kyser K., Thomas D., Polito P. and Marlat J. (2009a) Geochronology of
779 unconformity-related uranium deposits in the Athabasca Basin, Saskatchewan, Canada
780 and their integration in the evolution of the basin. *Miner. Deposita* **44**, 41–59.
781 Alexandre P., Kyser K. and Jiricka, D. (2009b) Critical geochemical and mineralogical
782 factors for the formation of unconformity-related uranium deposits: comparison
783 between barren and mineralized systems in the Athabasca Basin, Canada. *Econ. Geol*.
784 **104**, 413–435.
785 Alexandre P., Kyser K., Jiricka D. and Witt G. (2012) Formation and evolution of the
786 Centennial unconformity-related uranium deposit in the South-Central Athabasca
787 Basin, Canada. *Econ. Geol.* **107**, 385–400.
788 Annesley I. R., Madore C., and Portella P. (2005) Geology and thermotectonic evolution of
789 the western margin of the Trans-Hudson Orogen: Evidence from the eastern sub-
790 Athabasca basement, Saskatchewan. *Can. J. Earth Sci.* **42**, 573–597.
791 Armstrong R. L. and Ramaekers P. (1985) Sr isotopic study of Helikian sediment and diabase
792 dikes in the Athabasca Basin, northern Saskatchewan. *Can. J. Earth Sci.* **22**, 399–407.
793 Bertram M. A., MacKenzie F. T., Bishop F. C. and Bischoff W. D. (1991) Influence of
794 temperature on the stability of magnesian calcite. *Am. Mineral.* **76**, 1889–1896.
795 Boiron M. C., Cathelineau M. and Richard A. (2010) Fluid flows and metal deposition near
796 basement/cover unconformity: lessons and analogies from Pb-Zn-F-Ba systems for the
797 understanding of Proterozoic U deposits. *Geofluids* **10**, 270–292.
798 Bray C. J., Spooner E. T. C. and Longstaffe, F. J. (1988) Unconformity-related uranium
799 mineralization, McClean deposits, North Saskatchewan, Canada: Hydrogen and
800 oxygen isotope geochemistry. *Can. Mineral.* **26**, 249–268.

801 Burton E. A. and Walter L. M. (1991) The effects of $P_{CO2}$ and temperature on magnesium
802 incorporation in calcite in seawater and $MgCl_2$–$CaCl_2$ solutions. *Geochim. Cosmochim. Acta* **55**, 777–785.
804 Carignan J., Hild P., Mevelle G., Morel J. and Yeghicheyan D. (2001) Routine analyses of
805 trace elements in geological samples using flow injection and low pressure on-line
806 liquid chromatography coupled to ICP-MS: A study of geochemical reference
807 materials BR, DR-N, UB-N, AN-G and GH. *Geostandard Newslett.* **25**, 187–198.
808 Card C., Portella P., Annesley I. R. and Pana D. (2007) Basement rocks to the Athabasca
809 basin. *Bull. Geol. Surv. Can.* **588**, 69–87.
810 Carl C., Von Pechmann E., Hohndorf A., and Ruhrmann G. (1992) Mineralogy and U/Pb,
811 Pb/Pb, and Sm/Nd geochronology of the Key Lake uranium deposit, Athabasca Basin,
812 Saskatchewan, Canada. *Can. J. Earth Sci.* **29**, 879–895.
813 Chacko, T., Cole, D. R. and Horita, J. (2003) Equilibrium oxygen, hydrogen and carbon
814 isotope fractionation factors applicable to geologic systems. *Rev. Mineral. Geochem.*
815 **43**, 1–61.
816 Chiarenzelli J., Aspler L., Villeneuve M., and Lewry J. (1998) Early Proterozoic evolution of
817 the Saskatchewan craton and its allochtonous cover, Trans-Hudson orogen. *J. Geol.*
818 **106**, 247-267.
819 Clayton, R. N. and Mayeda, T. K. (1963) The use of bromine pentafluoride in the extraction
820 of oxygen from oxides and silicates for isotopic analysis. *Geochim. Cosmochim. Acta*
821 **27**, 43–52.
822 Cloutier J., Kyser K., Olivo G. R., Alexandre P. and Halaburda J. (2009) The Millennium
823 uranium deposit, Athabasca Basin, Saskatchewan, Canada: An atypical basement-
824 hosted unconformity-related uranium deposit. *Econ. Geol.* **104**, 815–840.

825 Cloutier J., Kyser K., Olivo G. R. and Alexandre, P. (2010) Contrasting patterns of alteration
826 at the Wheeler River area, Athabasca basin, Saskatchewan, Canada: Insights into the
827 apparently uranium-barren zone K alteration system. *Econ. Geol.* **105**, 303–324.
828 Cloutier J., Kyser K., Olivo G. and Brisbin D. (2011) Geochemical, isotopic, and
829 geochronologic constraints on the formation of the Eagle Point basement-hosted
830 uranium deposit, Athabasca Basin, Saskatchewan, Canada and recent remobilization
831 of primary uraninite in secondary structures. *Miner. Deposita* **46**, 35–56.
832 Conliffe J., Azmy K., Glesson S.A. and Lavoie D. (2010) Fluids associated with hydrothermal
833 dolomitization in St. George Group, western Newfoundland, Canada. *Geofluids* **10**,
834 422–437.
835 Cumming G. L. and Krstic D. (1992) The age of unconformity-related uranium mineralization
836 in the Athabasca Basin, northern Saskatchewan. *Can. J. Earth Sci.* **29**, 1623–1639.
837 Davisson M. L. and Criss R. E. (1996) Na-Ca-Cl relations in basinal fluids. *Geochim.*
838 *Cosmochim. Acta* **60**, 2743–2752.
839 Derome D., Cathelineau M., Lhomme T. and Cuney M. (2003a) Fluid inclusion evidence of
840 the differential migration of $H_2$ and $O_2$ in the McArthur River unconformity-type
841 uranium deposit (Saskatchewan, Canada). Possible role on post-ore modifications of
842 the host rocks. *J. Geochem. Explor.* **78-79**, 525–530.
843 Derome D., Cuney M., Cathelineau M., Fabre C., Dubessy J., Bruneton P. and Hubert A.
844 (2003b) A detailed fluid inclusion study in silicified breccias from the Kombolgie
845 sandstones (Northern Territory, Australia): Inferences for the genesis of middle-
846 Proterozoic unconformity-type uranium deposits. *J. Geochem. Explor.* **80**, 259–275.
847 Derome D., Cathelineau M., Cuney M., Fabre C., Lhomme T. and Banks D. A. (2005) Mixing
848 of sodic and calcic brines and uranium deposition at McArthur River, Saskatchewan,

849 Canada: A Raman and laser-induced breakdown spectroscopic study of fluid
850 inclusions. *Econ. Geol.* **100**, 1529–1545.
851 Derome D., Cathelineau M., Fabre C., Boiron, M. C., Banks D., Lhomme T., Cuney M.
852 (2007) Paleo-fluid composition determined from individual fluid inclusions by Raman
853 and LIBS: Application to mid-proterozoic evaporitic Na-Ca brines (Alligator Rivers
854 Uranium Field, northern territories Australia). *Chem. Geol.* **237**, 240–254.
855 Derry L. A. and Jacobsen S. B. (1988) The Nd and Sr isotopic evolution of Proterozoic
856 seawater. *Geophys. Res. Lett.* **15**, 397–400.
857 Dubessy J., Pagel M., Beny J. M., Christensen H., Hickel B., Kosztolanyi C. and Poty, B.
858 (1988) Radiolysis evidenced by $H_2$-$O_2$ and $H_2$-bearing fluid inclusions in three
859 uranium deposits. *Geochim. Cosmochim. Acta* **52**, 1155–1167.
860 Dubois M. and Marignac C. (1997) The $H_2O$-NaCl-$MgCl_2$ ternary phase diagram with special
861 application to fluid inclusion studies. *Econ. Geol.* **92**, 114–119.
862 Eslinger E. V. and Savin S. M. (1973) Mineralogy and oxygen isotope geochemistry of the
863 hydrothermally altered rocks of the Ohaki-Broadlands, New Zealand geothermal area.
864 *Am. J. Sci.* **273**, 240–270.
865 Essarraj S., Boiron M. C., Cathelineau M., Banks D. A. and Benharref M. (2005) Penetration
866 of surface-evaporated brines into the Proterozoic basement and deposition of Co and
867 Ag at Bou Azzer (Morrocco): Evidence from fluid inclusions. *J. Afr. Earth Sci.* **41,**
868 25–39.
869 Fayek M. and Kyser T. K. (1997) Characterization of multiple fluid-flow events and rare-
870 earth-element mobility associated with formation of unconformity-type uranium
871 deposits in the Athabasca Basin, Saskatchewan. *Can. Mineral.* **35**, 627–658.

872 Fayek M., Harrison T. M., Ewing R. C., Grove M. and Coath C. D. (2002) O and Pb isotopic
873 analyses of uranium minerals by ion microprobe and U-Pb ages from the Cigar Lake
874 deposit. *Chem. Geol.* **185**, 205–225.
875 Fryer B. J. and Taylor R. P. (1984) Sm-Nd direct dating of the Collins Bay hydrothermal
876 uranium deposit, Saskatchewan. *Geology* **12**, 479–482.
877 Gaboreau S., Cuney M., Quirt D., Beaufort D., Patrier P. and Mathieu R. (2007) Significance
878 of aluminum phosphate-sulfate minerals associated with U unconformity-type
879 deposits: The Athabasca basin, Canada. *Am. Mineral.* **92**, 267–280.
880 Genest S., Robert F. and Duhamel I. (2010) The Carswell impact event, Saskatchewan,
881 Canada: Evidence for a pre-Athabasca multiring basin? *Geol. S. Am. S.* **465**, 543–570.
882 Gleeson S. A., Wilkinson, J. J., Boyce A. J., Fallick A. E. and Stuart F. M. (1999) On the
883 occurrence and wider implications of anomalously low δD fluids in quartz veins,
884 South Cornwall, England. *Chem. Geol.* **160**, 161–173.
885 Gleeson S.A. and Turner W.A. (2007) Fluid inclusion constraints on the origin of the brines
886 responsible for Pb–Zn mineralization at Pine Point and coarse non-saddle and saddle
887 dolomite formation in southern Northwest Territories. *Geofluids* **7**, 51–68.
888 Gleeson S. A., Roberts S., Fallick A. E. and Boyce A. J. (2008) Micro-Fourier Transform
889 Infrared (FT-IR) and δD value investigation of hydrothermal vein quartz:
890 Interpretation of fluid inclusion δD values in hydrothermal systems. *Geochim.*
891 *Cosmochim. Acta* **72**, 4595–4606.
892 Gromek P., Gleeson S.A. and Simonetti A. (2012) A basement-interacted fluid in the N81
893 deposit, Pine Point Pb-Zn District, Canada: Sr isotopic analyses of single dolomite
894 crystals. *Miner. Deposita* **47**, 749–754.

895 Halter G., Sheppard S. M. F., Weber F., Clauer N. and Pagel M. (1987) Radiation-related
896 retrograde hydrogen isotope and K-Ar exchange in clay minerals. *Nature* **330**, 638–
897 641.
898 Hecht L. and Cuney M. (2000) Hydrothermal alternation of monazite in the Precambrian
899 crystalline basement of the Athabasca Basin (Saskatchewan, Canada): Implications for
900 the formation of unconformity-related uranium deposits. *Miner. Deposita* **35**, 791–
901 795.
902 Heine T. H. (1986) The geology of the Rabbit Lake uranium deposit, Saskatchewan. In
903 *Uranium deposits of Canada. Canadian institute of Mining, Metallurgy and*
904 *Petroleum, Special Volume 33* (ed. E. L. Evans). pp. 134–143.
905 Hoeve J. and Sibbald T. I. I. (1978) On the genesis of the Rabbit Lake and other
906 unconformity-type uranium deposits in Northern Saskatchewan, Canada. *Econ. Geol.*
907 **73**, 1450–1473.
908 Hoeve J. and Quirt D. (1987) A stationary redox front as a critical factor in the formation of
909 high-grade, unconformity-type uranium ores in the Athabasca Basin, Saskatchewan,
910 Canada. *Bull. Mineral.* **110**, 151–171.
911 Hoeve J., Kyser T. K. and Forester R. W. (1986) Cover-basement interaction and the origin of
912 U-Ni-Co mineralization in the Athabsca Basin: Isotopic evidence (O, H, C).
913 *Saskatchewan Research Council Publication No. R-855-3-A-86*. 89 pp.
914 Hoffman P. (1990) Subdivision of the Churchill Province and extent of the Trans-Hudson
915 Orogen. In *The Early Proterozoic Trans-Hudson Orogen of North America.*
916 *Geological Association of Canada Special Paper 37* (eds. J. F. Lewry and M. R.). pp.
917 15–39.
918 Holser W. (1979) Trace elements and isotopes in evaporites. *Rev. Mineral.* **6**, 295–346.

Houston S., Smalley C., Laycock A. and Yardley B. W. D. (2011) The relative importance of buffering and brine inputs in controlling the abundance of Na and Ca in sedimentary formation waters. *Mar. Petrol. Geol.* **28**, 1242–1251.

Jaffrés J.B.D., Shields G.A. and Wallmann K. (2007) The oxygen isotope evolution of seawater: A critical review of a long-standing controversy and an improved geological water cycle model for the past 3.4 billion years. *Earth-Sci. Rev.* **83**, 83–122.

Jefferson C. W., Thomas D. J., Gandhi S. S., Ramaekers P., Delaney G., Brisbin D., Cutts C., Portella P. and Olson R. A. (2007) Unconformity associated uranium deposits of the Athabasca Basin, Saskatchewan and Alberta. *Bull. Geol. Surv. Can.* **588**, 23–67.

Kesler S. E., Appold M. S., Martini A. M., Walter L. M., Huston T. J. and Kyle J. R. (1995) Na-Cl-Br systematics of mineralizing brines in Mississippi Valley-type deposits. *Geology* **23**, 641–644.

Knauth L. P. and Beeunas M. A. (1986) Isotope geochemistry of fluid inclusions in Permian halite with implications for the isotopic history of ocean water and the origin of saline formation waters. *Geochim. Cosmochim. Acta* **50**, 419–433.

Kotzer T. G. and Kyser T. K. (1991) Retrograde alteration of clay minerals in uranium deposits: radiation-catalysed or simply low-temperature exchange? *Chem. Geol.* **86**, 307–321.

Kotzer T. G., Kyser T. K., King R. W. and Kerrich R. (1993) An empirical oxygen- and hydrogen-isotope geothermometer for quartz-tourmaline and tourmaline-water, *Geochim. Cosmochim. Acta* **57**, 3421–3426.

Kotzer T. G. and Kyser T. K. (1995) Petrogenesis of the Proterozoic Athabasca Basin, Northern Saskatchewan, Canada, and its relation to diagenesis, hydrothermal uranium mineralization and paleohydrogeology. *Chem. Geol.* **120**, 45–89.

943 Kyser T. K., Wilson M. R. and Ruhrmann G. (1989) Stable isotope constraints on the role of
944 graphite in the genesis of unconformity-type uranium deposits. *Can. J. Earth Sci.* **26**,
945 490–498.
946 Kyser T. K. and Kerrich R. (1990) Geochemistry of fluids in tectonically active crustal
947 regions. In *Fluids in teconically active regimes of the continental crust. Mineralogical*
948 *Association of Canada Short Course Series*, vol. 18 (ed. E. Nesbitt). pp. 133–230.
949 Kyser T. K., Hiatt E., Renac C., Durocher K., Holk G., Deckart K. (2000) Diagenetic fluids in
950 Paleo- and Meso-Proterozoic sedimentary basins and their implications for long
951 protracted fluid histories. In *Fluids and basin evolution, Mineralogical association of*
952 *Canada Short Course Series 28* (ed. K. Kyser). pp. 225–262.
953 Kyser T. K. and Cuney M. (2008) Unconformity-related uranium deposits. In *Recent and Not-*
954 *So-Recent Developments in Uranium Deposits and Implications for Exploration.*
955 *Mineralogical Association of Canada Short Course Series 39* (eds M. Cuney and K.
956 Kyser). pp. 161–219.
957 Landais P. and Dereppe J. M. (1985) A chemical study of the carbonaceous material from the
958 Carswell Structure. In *The Carswell Structure Uranium Deposits, Saskatchewan.*
959 *Geological Association of Canada Special Paper, vol 29,* (eds. R. Lainé, D. Alonso
960 and M. Svab). pp. 165–174.
961 Landais P., Dubessy J., Poty B. and Robb L. J. (1990) Three examples illustrating the analysis
962 of organic matter associated with uranium ores. *Org. Geochem.* **16**, 601–608.
963 Landais P., Dubessy J., Dereppe J. M. and Philp R. P. (1993) Characterization of graphite
964 alteration and bitumen genesis in the Cigar Lake deposit (Saskatchewan, Canada).
965 *Can. J. Earth Sci.* **30**, 743–753.
966 Landais P. (1996) Organic geochemistry of sedimentary uranium ore deposits. *Ore Geol. Rev.*
967 **11**, 33–51.

968 Laverret E., Patrier Mas P., Beaufort D., Kister P., Quirt D., Bruneton P. and Clauer N. (2006)
969 Mineralogy and geochemistry of the host-rock alterations associated with the Shea
970 Creek unconformity-type uranium deposits (Athabasca Basin, Saskatchewan, Canada).
971 Part 1. Spatial variation of illite properties. *Clay. Clay. Miner.* **54**, 275–294.
972 Laverret E., Clauer N., Fallick A., Mercadier J., Patrier P., Beaufort D., Bruneton P. (2010)
973 K-Ar dating and $\delta^{18}O$-$\delta D$ tracing of illitization within and outside the Shea Creek
974 uranium prospect, Athabasca Basin, Canada. *Appl. Geochem.* **25**, 856–871.
975 Le Carlier de Veslud C., Cuney M., Lorilleux G., Royer J. J. and Jébrak M. (2009) 3D
976 modeling of uranium-bearing solution-collapse breccias in Proterozoic sandstones
977 (Athabasca Basin, Canada) - Metallogenic interpretations. *Comput. Geosci.* **35**, 92–
978 107.
979 Lécuyer C., Gruau G., Früh-Green G.L. and Picard C. (1996) Hydrogen isotope composition
980 of Early Proterozoic seawater. *Geology* **24**, 291–294.
981 Leisen M., Boiron M.C., Richard A. and Dubessy J. (2012) Determination of Cl and Br
982 concentrations in individual fluid inclusions by combining microthermometry and LA-
983 ICPMS analysis: Implications for the origin of salinity in crustal fluids. *Chem. Geol.*
984 **330–331**, 197–206.
985 Leventhal J. S., Grauch R. I., Threlkeld C. N., Lichte F. E. and Harper C. T. (1987) Unusual
986 organic matter associated with uranium from the Claude deposit, Cluff Lake, Canada.
987 *Econ. Geol.* **82**, 1169–1176.
988 Lin L. H., Slater G. F., Sherwood Lollar B., Lacrampe-Couloume G. and Onstott, T. C.
989 (2005) The yield and isotopic composition of radiolytic $H_2$, a potential energy source
990 for the deep subsurface biosphere. *Geochim. Cosmochim. Acta* **69**, 893–903.

991 Lopez O., Zuddas P. and Faivre D. (2009) The influence of temperature and seawater
992 composition on calcite crystal growth mechanisms and kinetics: Implications for Mg
993 incorporation in calcite lattice. *Geochim. Cosmochim. Acta* **73**, 337–347.
994 Lorilleux G., Jébrak M., Cuney M. and Baudemont D. (2002) Polyphase hydrothermal breccia
995 associated with unconformity-related uranium mineralizations (Canada). From fractal
996 analysis to structural significance. *J. Struct. Geol.* **24**, 223–238.
997 Lorilleux G., Cuney M., Jébrak M., Rippert J. C. and Portella P. (2003) Chemical brecciation
998 processes in the Sue unconformity-type uranium deposits, Eastern Athabasca Basin
999 (Canada). *J. Geochem. Explor.* **80**, 241–258.
1000 Luais B., Telouk P. and Albarède F. (1997) Precise and accurate neodymium isotopic
1001 measurements by plasma-source mass spectrometry. *Geochim. Cosmochim. Acta* **61**,
1002 4847–4854.
1003 McCrea, J. M. (1950) On the isotope chemistry of carbonates and a paleotemperature scale. *J.*
1004 *Chem. Phys.* **18**, 849–857.
1005 McCready A. J., Annesley, I. R., Parnell, J. and Richardson, L. C. (1999) Uranium-bearing
1006 carbonaceous matter, McArthur River uranium ore-deposit, Saskatchewan.
1007 *Saskatchewan Geological Survey, Saskatchewan Energy and Mines, Summary of*
1008 *Investigations* **1999-2**, 110–120.
1009 McCready A. J., Annesley I. R., Rickers K. and Cavell R. G. (2007) First insights into the
1010 inorganic chemistry of 'carbon phases' from basement rocks to uranium deposits in
1011 the Athabasca Basin, Canada. In *Proceedings of the Ninth Biennial SGA Meeting,*
1012 *Digging Deeper* (eds. C. J. Andrew et al.). Dublin, Ireland. pp. 1145–1148.
1013 Mercadier J., Richard A., Boiron M. C., Cathelineau M. and Cuney M. (2010) Brine
1014 migration in the basement rocks of the Athabasca Basin through microfracture
1015 networks (P-Patch U deposit, Canada). *Lithos* **115**, 121–136.

1016 Mercadier J., Cuney M., Lach P., Boiron M. C., Bonhoure J., Richard A., Leisen M. and
1017 Kister P. (2011a) Origin of uranium deposits revealed by their rare earth element
1018 signature. *Terra Nova* **23**, 264–269.
1019 Mercadier J., Cuney M., Cathelineau M. and Lacorde M. (2011b) U redox fronts and
1020 kaolinisation in basement-hosted unconformity-related U ores of the Athabasca Basin
1021 (Canada): late U remobilisation by meteoric fluids. *Miner. Deposita* **46**, 105–135.
1022 Mercadier J., Richard A. and Cathelineau M. (2012) Boron and magnesium-rich marine
1023 brines at the origin of giant unconformity-related uranium deposits: $\delta^{11}B$ evidence
1024 from Mg-tourmalines. *Geology* **40**, 231–234.
1025 Mercadier J., Annesley I. R., McKechnie C. L., Bogdam T. and Creighton S. (2013)
1026 Magmatic and metamorphic uranium mineralization in the western margin of the
1027 Trans-Hudson Orogen (Saskatchewan, Canada): a metal source for unconformity-
1028 related uranium deposits? *Economic Geology*, in press.
1029 Muchez P., Heijlen W., Banks D. A., Blundell D., Boni M. and Grandia F. (2005) Extensional
1030 tectonics and the timing and formation of basin-hosted deposits in Europe. *Ore Geol.*
1031 *Rev.* **27**, 241–267.
1032 Ohmoto H. and Rye R. O. (1979) Isotope of sulfur and carbon. In *Geochemistry of*
1033 *Hydrothermal deposits* (ed. H. L. Barnes). John Wiley & Sons, pp. 509-567.
1034 Pagel M. (1975) Détermination des conditions physico-chimiques de la silicification
1035 diagénétique des grès Athabasca (Canada) au moyen des inclusions fluides. *C. R.*
1036 *Acad. Sc. Paris* **280**, 2301–2304.
1037 Pagel M., Poty B. and Sheppard S. M. F. (1980) Contribution to some Saskatchewan uranium
1038 deposits mainly from fluid inclusion and isotopic data. In *International Uranium*
1039 *Symposium on the Pine Creek Geosyncline* (eds. J. Ferguson and A. Goleby). IAEA,
1040 Vienna. pp. 639–654.

1041 Pagel M., Wheatley K. and Ey F. (1985) Origin of the Carswell circular structure. A summary
1042 of data for geological interpretation of its formation. In *The Carswell Structure*
1043 *Uranium Deposits Saskatchewan, Geological Association of Canada Special Paper 29*
1044 (eds. R. Laine, D. Alonso, M. Svab.). pp. 213–223.
1045 Pagel M., Michard A., Juteau M. and Turpin L. (1993) Sm-Nd, Pb-Pb, and Rb-Sr systematics
1046 of the basement in the Cigar Lake area, Saskatchewan, Canada. *Can. J. Earth Sci.* **30**,
1047 731–742.
1048 Percival J. B., Bell K. and Torrance J. K. (1993) Clay mineralogy and isotope geochemistry
1049 of the alteration halo at the Cigar Lake uranium deposit. *Can. J. Earth Sci.* **30**, 689–
1050 704.
1051 Pettke T., Audétat A., Schaltegger U. and Heinrich C. A. (2005) Magmatic-to-hydrothermal
1052 crystallization in the W–Sn mineralized Mole Granite (NSW, Australia) Part II:
1053 Evolving zircon and thorite trace element chemistry. *Chem. Geol.* **220**, 191–213.
1054 Pin C., Briot D., Bassin C. and Poitrasson F. (1994) Concomitant separation of strontium and
1055 samarium-neodymium for isotopic analysis in silicate samples, based on specific
1056 extraction chromatography. *Anal. Chim. Acta* **298**, 209–217.
1057 Pin C. and Santos Zalduegui J. F. (1997) Sequential separation of light rare-earth elements,
1058 thorium and uranium by miniaturized extraction chromatography: Application to
1059 isotopic analyses of silicate rocks. *Anal. Chim. Acta* **339**, 79–89.
1060 Pope E.C., Bird D.K. and Rosing M.T. (2012) Isotope composition and volume of Earth's
1061 early oceans. *P. Natl. Acad. Sci. USA.* **109**, 4371–4376..
1062 Ramaekers P., Jefferson C. W., Yeo G. M., Collier B., Long D. G., Catuneanu O., Bernier S.,
1063 Kupsch B., Post R., Drever G., McHardy S., Jircka D., Cutts C. and Wheatley K.
1064 (2007) Revised geological map and stratigraphy of the Athabasca Group,
1065 Saskatchewan and Alberta. *Bull. Geol. Surv. Can.* **588,** 155–191.

1066 Rasmussen B., Buick R. and Taylor W. R. (1998) Removal of oceanic REE by authigenic
1067 precipitation of phosphatic minerals. *Earth Planet. Sci. Lett.* **164** (1998) 135–149.
1068 Richard A., Pettke T., Cathelineau M., Boiron M. C., Mercadier J., Cuney M. and Derome, D.
1069 (2010) Brine-rock interaction in the Athabasca basement (McArthur River U deposit,
1070 Canada): consequences for fluid chemistry and uranium uptake. *Terra Nova* **22**, 303–
1071 308.
1072 Richard A., Banks D. A., Mercadier J., Boiron M. C., Cuney M., and Cathelineau M. (2011)
1073 An evaporated seawater origin for the ore-forming brines in unconformity-related
1074 uranium deposits (Athabasca Basin, Canada): Cl/Br and $\delta^{37}$Cl study of fluid
1075 inclusions. *Geochim. Cosmochim. Acta* **75**, 2792–2810.
1076 Richard A, Rozsypal C., Mercadier J., Banks D. A., Cuney M., Boiron M. C. and Cathelineau
1077 M. (2012) Giant uranium deposits formed from exceptionally uranium-rich acidic
1078 brines. *Nat. Geosci.* **5**, 142–146.
1079 Richard A., Cauzid J., Cathelineau M., Boiron M.C., Mercadier J. and Cuney M. (2013)
1080 Synchrotron-XRF and XANES investigation of uranium speciation and element
1081 distribution in fluid inclusions from unconformity-related uranium deposits.
1082 *Geofluids*, in press, doi: 10.1111/gfl.12009.
1083 Rosenbaum J. and Sheppard S.M. (1986) An isotopic study of siderites, dolomites and
1084 ankerites at high temperatures. *Geochim. Cosmochim. Acta* **50**, 1147–1150.
1085 Sangély L., Chaussidon M., Michels R., Brouand M., Cuney M., Huault V. and Landais P.
1086 (2007) Micrometer scale carbon isotopic study of bitumen associated with Athabasca
1087 uranium deposits: Constraints on the genetic relationship with petroleum source-rocks
1088 and the abiogenic origin hypothesis. *Earth Planet. Sci. Lett.* **258**, 378–396.

1089 Savary V. and Pagel M. (1997) The effects of water radiolysis on local redox conditions in the
1090 Oklo, Gabon, natural fission reactors 10 and 16. *Geochim. Cosmochim. Acta* **61**,
1091 4479–4494.
1092 Sheppard S. M. F. (1986) Characterization and isotopic variations in natural waters. *Rev.*
1093 *Mineral.* **16**, 165–183.
1094 Shields G. and Veizer J. (2002) Precambrian marine carbonate isotope database: Version 1.1.
1095 *Geochem. Geophy. Geosy.* **3**, U1–U12.
1096 Simon K. (2001) Does δD from fluid inclusion in quartz reflect the original hydrothermal
1097 fluid? *Chem. Geol.* **177**, 483–495.
1098 Steele-MacInnis M., Bodnar R.J. and Naden J. (2011) Numerical model to determine the
1099 composition of $H_2O$-NaCl-$CaCl_2$ fluid inclusions based on microthermometric and
1100 microanalytical data. *Geochim. Cosmochim. Acta* **75**, 21–40.
1101 Taylor S. R. and McLennan S. M. (1985) The Continental Crust: Its Composition and
1102 Evolution. Blackwell, Oxford. 312 p.
1103 Veizer J. (1989) Strontium isotopes in seawater though time. *Ann. Rev. Earth Planet. Sci.* **17**,
1104 141–167.
1105 Wallis R. H., Saracoglu N., Brummer J. J. and Golightly J. P. (1984) The geology of the
1106 McClean uranium deposits, northern Saskatchewan. In *Geology of Uranium Deposits -*
1107 *Canadian Institute of Mining, Metallurgy and Petroleum Special Volume 32*. pp. 101–
1108 131.
1109 Wang A., Dhamelincourt P., Dubessy J., Guerard D., Landais P. and Lelaurain M. (1989)
1110 Characterization of graphite alteration in an uranium deposit by micro-Raman
1111 spectroscopy, X-ray diffraction, transmission electron microscopy and scanning
1112 electron microscopy. *Carbon* **27**, 209–218.

1113 Warren J. (2000) Dolomite: occurrence, evolution and economically important associations.
1114 *Earth-Sci. Rev.* **52**, 1–81.
1115 Wenner D. B. and Taylor H. P. Jr. (1971) Temperatures of serpentinization of ultramafic
1116 rocks based on $^{18}O/^{16}O$ fractionation between coexisting serpentine and magnetite.
1117 *Contrib. Mineral. Petrol.* **32**, 165–185.
1118 Williams A. E. and McKibben M. A. (1989) A brine interface in the Salton Sea Geothermal
1119 System, California: Fluid geochemical and isotopic characteristics. *Geochim.*
1120 *Cosmochim. Acta* **53**, 1905–1920.
1121 Wilson M. R. and Kyser T. K. (1987) Stable isotope geochemistry of alteration associated
1122 with the Key Lake uranium deposit, Canada. *Econ. Geol.* **82**, 1540–1557.
1123 Wilson M. R., Kyser T. K., Mehnert H. H. and Hoeve J. (1987) Changes in the H-O-Ar
1124 isotope composition of clays during retrograde alteration. *Geochim. Cosmochim. Acta*
1125 **51**, 869–878.
1126 Wilson N. S. F., Stasiuk L. D., and Fowler M. G. (2007) Origin of organic matter in the
1127 Proterozoic Athabasca Basin of Saskatchewan and Alberta, and significance to
1128 unconformity uranium deposits. *Bull. Geol. Surv. Can.* **588**, 325–339.
1129 Zhang J. and Nozaki Y., (1998) Behavior of rare earth elements in seawater at the ocean
1130 margin: A study along the slopes of the Sagami and Nankai troughs near Japan.
1131 *Geochim. Cosmochim. Acta* **62**, 1307–1317.
1132 Zheng Y. F. (1993a) Calculation of oxygen isotope fractionation in anhydrous silicate
1133 minerals. *Geochim. Cosmochim. Acta* **57**, 1079–1091.
1134 Zheng Y. F. (1993b) Calculation of oxygen isotope fractionation in hydroxyl-bearing
1135 silicates. *Earth Planet. Sci. Lett.* **120**, 247–263.
1136 Zheng Y. F. (1999) Oxygen isotope fractionation in carbonate and sulfate minerals. *Geochem.*
1137 *J.* **33**, 109–129.

**Table captions**

Table 1: O, H (vs. V-SMOW), C (vs. V-PDB) composition of quartz and dolomite veins and their fluid inclusions from Athabasca Basin and Basement, with location and petrographic description. U/C: unconformity (negative depths indicate that samples were taken in the sandstones). When the depth is unknown, sst and bst indicate that the samples were taken in the sandstones or in the basement respectively. Mineral and rock abbreviations: Qtz: quartz; Dol; dolomite; Hem: hematite; Drv: dravite; Ill: Illite; Chl: chlorite; Pegm: pegmatoid. "Bleached" stands for samples altered to illite-chlorite-dravite±quartz assemblages.

Table 2: Major and trace element data on dolomite veins. LOI: loss on ignition.

Table 3: Rb/Sr and Sm/Nd isotope data for dolomite veins. $^{87}Rb/^{86}Sr$ ratios for samples with Rb concentration below 0.3 ppm were calculated using Rb concentration of 0.15 ppm. This results in calculated $^{87}Sr/^{86}Sr_i$ values nearly indistinct from the today $^{87}Sr/^{86}Sr$. Therefore for these samples $^{87}Sr/^{86}Sr_i$ values are not reported. The Nd isotope composition of MAC5 sample was not measured due to insufficient Nd content.

**Figure captions**

Fig. 1: (A) Simplified geological map of the Athabasca Basin and its underlying Rae and Hearne Subprovinces, with location of the six studied unconformity-related U deposits (full stars) (modified from Card et al. (2007) and Jefferson et al. (2007)). Cigar Lake

1163 deposit (empty star) was not studied here but is mentioned in the text. (B) Simplified
1164 mineral paragenesis for unconformity-related U deposits in the Athabasca Basin. The
1165 type of alteration (E: early diagenetic, hydrothermal and late meteoric), their
1166 temperature and timing are indicated. Diag.: diagenetic. Modified from Kotzer and
1167 Kyser (1995), Derome et al. (2005), Kyser and Cuney (2008) and Mercadier et al.
1168 (2011b).
1169
1170 Fig. 2: Examples of quartz and dolomite veins and their fluid inclusions studied in this work.
1171 (A) Quartz and quartz-hematite veins crosscutting a hematite-rich gneiss (sample
1172 ERC5-922.0, Shea Creek). (B) Hematite-dolomite vein crosscutting a biotite-rich
1173 gneiss (sample H1935-8, Eagle Point). (C) Quartz-dolomite vein crosscutting a
1174 hematite-rich gneiss (sample RBL2, Rabbit Lake). (D) Quartz-dolomite vein
1175 crosscutting "bleached" (illite-chlorite-dravite alteration) gneiss (sample CX52-1,
1176 Millennium). (E) Close up on one quartz vein showing multiple individual quartz
1177 crystals (view on thick section, sample RBL2, Rabbit Lake). (F) Close up on one
1178 dolomite vein showing multiple individual dolomite crystals (view on thick section,
1179 sample RBL2, Rabbit Lake). (G) Primary two-phase (liquid + vapor) and three-phase
1180 (liquid + vapor + halite) fluid inclusions at room temperature, typically found in quartz
1181 (as shown here) and dolomite veins. Further illustration of fluid inclusions and quartz-
1182 dolomite veins, can be found in Pagel et al., 1980; Kotzer and Kyser, 1995; Derome et
1183 al., 2005; Richard et al., 2010, 2011, 2012). For an example of quartz-dolomite vein in
1184 mineralized samples see detailed description of sample MAC5 in Derome et al.
1185 (2005), referred as sample H459-33.
1186

Fig. 3 : O, H, C isotope composition of quartz-dolomite veins and their fluid inclusions in the Athabasca Basin and Basement. (A) $\delta^{18}O$ values of quartz and dolomite veins, compared with the $\delta^{18}O$ values of alteration minerals (illite, chlorite and dravite) around unconformity-related U deposits in the Athabasca Basin (see Section 5.1.2. for details and source data for alteration minerals). The theoretical $\delta^{18}O$ values of quartz in isotopic equilibrium with illite, chlorite and dravite at 180°C are indicated (See Section 5.1.2 for fractionation factors). *(1)* Data from Rabbit Lake (n= 7) after Hoeve et al. (1986). *(2)* Data from Key Lake (n = 5) after Wilson and Kyser, (1987). *(3)* Data from McArthur River (n = 15) after Kotzer and Kyser (1995). The virtual $\delta^{18}O$ values of dolomite in isotopic equilibrium with the quartz veins studied here are also indicated (after Zheng, 1993a, 1999). (B) δD of water from quartz- and dolomite-hosted fluid inclusions. *(1)* Data from McArthur River (number of data not provided) after Kotzer and Kyser (1995). *(2)* Data from Rabbit Lake (n = 1) after Pagel et al. (1980). *(3)* Data from Rabbit Lake (n = 3) after Pagel et al. (1980). (C) $\delta^{18}O$ vs. $\delta^{13}C$ diagram for dolomite veins. *(1)* $\delta^{18}O$ vs. $\delta^{13}C$ from Rabbit Lake deposit (n = 40) after Pagel et al. (1980) and Hoeve et al. (1986). Field for Proterozoic marine carbonates after Shields and Veizer (2002). $\delta^{13}C$ range for graphite in Athabasca basement after Wallis et al. (1984) and Kyser et al. (1989). $\delta^{13}C$ range for bitumen in Athabasca unconformity-related U-ores after Sangély et al. (2007) and Hoeve et al. (1986).

Fig. 4: Rare Earth Element (REE) concentrations in Athabasca dolomite veins and other reference materials ($UO_2$, seawater, monazite, zircon, florencite). All data normalized to Post Archean Australian Shales (PAAS). Normalization values are from Taylor and McLennan (1988). Data is not shown for sample MAC5 which has very low REE abundances compared to other samples (see Table 1). Data for Athabasca $UO_2$

(McArthur River deposit) are indicated for comparison (after Mercadier et al., 2011a). Data for seawater after Zhang and Nozaki (1998); monazite and zircon after Pettke et al. (2005) and florencite (aluminum phosphate-sulphate mineral) after Rasmussen et al. (1998).

Fig. 5: Sr and Nd isotope compositions of the Athabasca dolomite veins. $^{87}Sr/^{86}Sr_i$ = $^{87}Sr/^{86}Sr$ for samples with Rb < 0.3 ppm (see Table 3). Compositional fields for reservoirs of interest have been reconstructed after data from various localities in the Athabasca basin and basement: (1) Proterozoic seawater (Derry and Jacobsen, 1988; Veizer, 1989); (2) Athabasca sandstones (Manitou Falls and Wolverine Point formations, Armstrong and Ramaekers, 1985; Pagel et al., 1993; Kotzer and Kyser (1995); (3) $UO_2$ (Fryer and Taylor, 1984; Carl et al., 1992; Pagel et al., 1993; Fayek and Kyser, 1997); Basement metapelites (Pagel et al., 1993).

Fig. 6: δD vs. $\delta^{18}O$ for fluid inclusion water in Athabasca quartz (diamonds) and dolomite (circles) veins. $\delta^{18}O$ values for fluid inclusion water were calculated assuming host mineral precipitation occurred at 180°C (quartz and dolomite with $\delta^{18}O$ < 19‰) and 120°C (dolomite with $\delta^{18}O$ > 19‰) (see Section 5.2.1. for details on reconstruction of $\delta^{18}O$ values). Seawater evaporation trend after Holser (1979) and Knauth and Beeunas (1986). *GMWL*: Global meteoric water line. *(1)* Representative fluid inclusion data from McArthur River quartz veins after Kotzer and Kyser (1995) ($\delta^{18}O$ values calculated from $\delta^{18}O$ values of host quartz at 180°C). *(2)* Fluid inclusion data from Rabbit Lake dolomite veins after Pagel et al. (1980) ($\delta^{18}O$ values calculated from $\delta^{18}O$ values of host dolomite at 180°C).

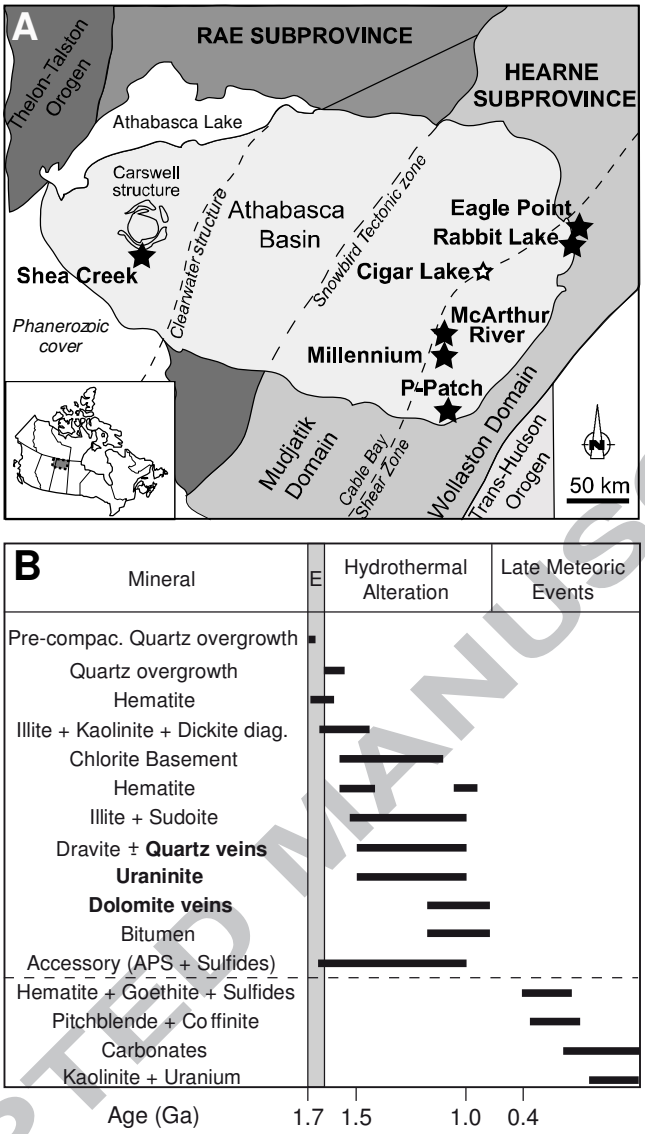


**FIGURE 1**

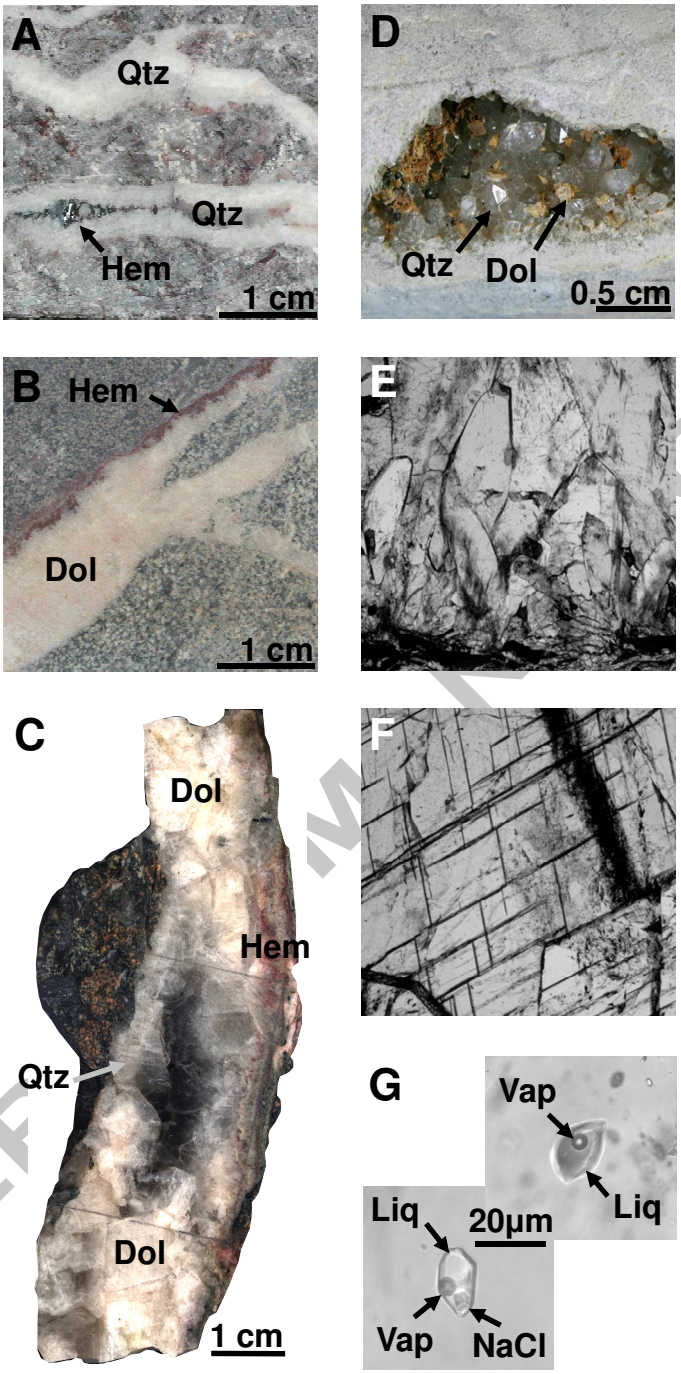


**FIGURE 2**

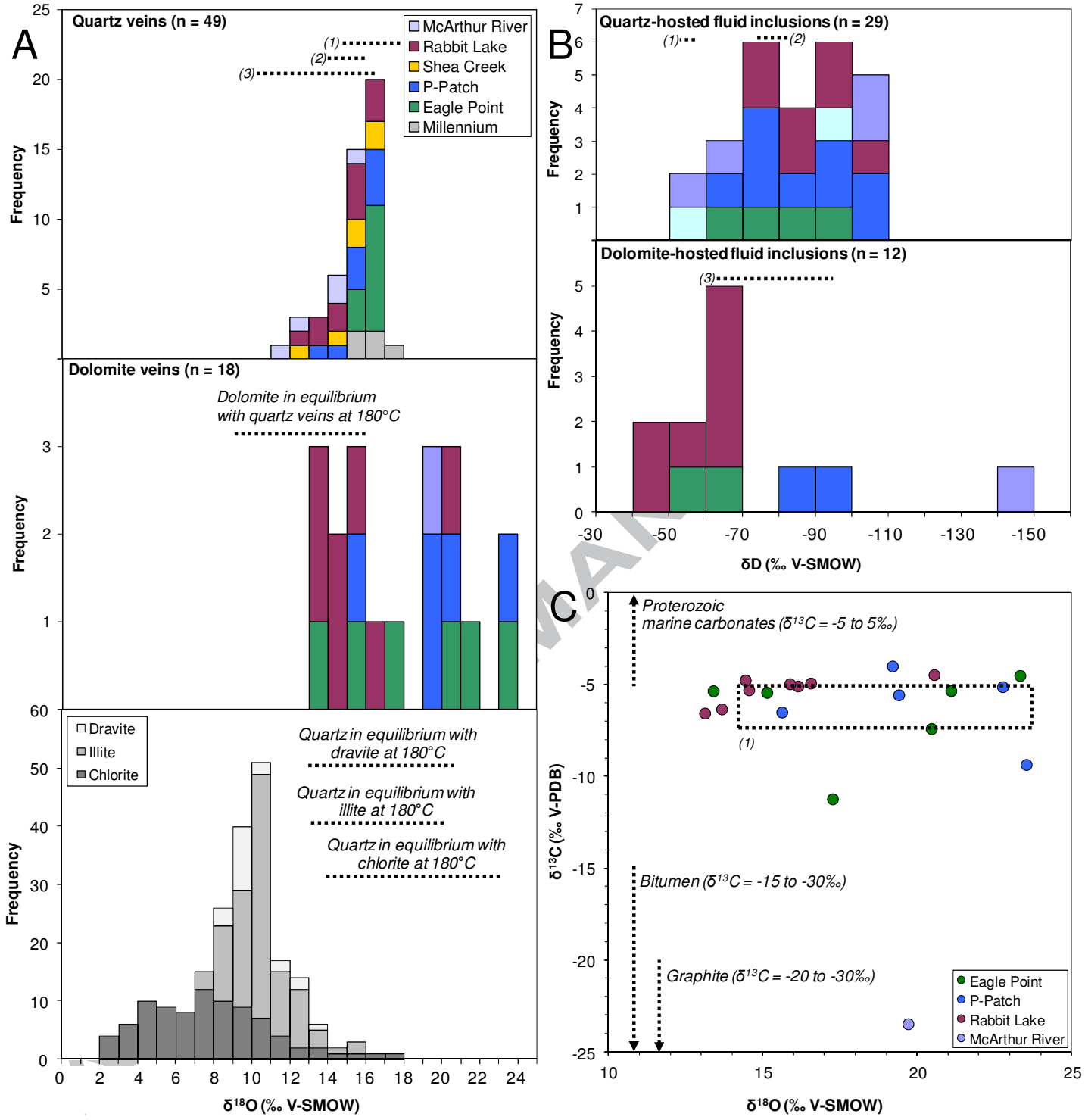


**FIGURE 3**

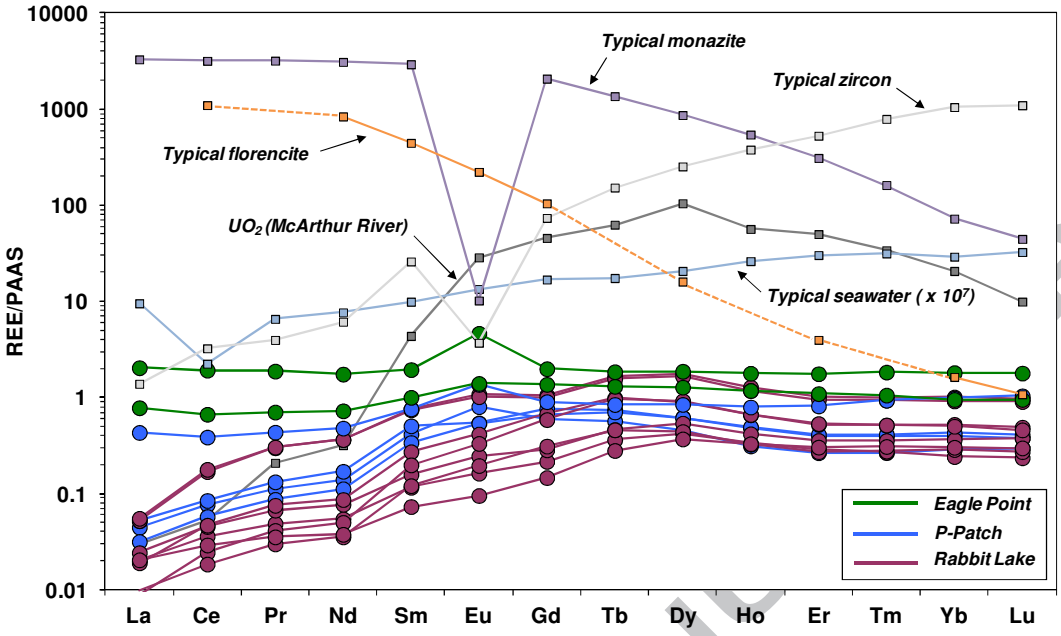


**FIGURE 4**

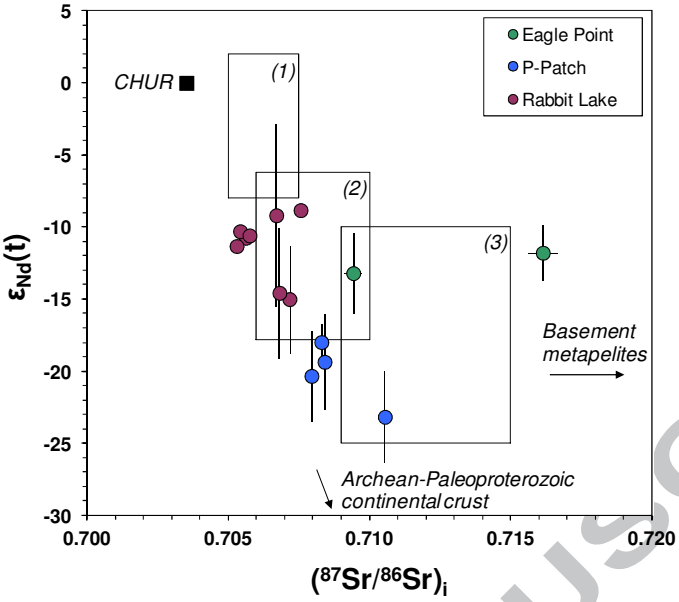


**FIGURE 5**

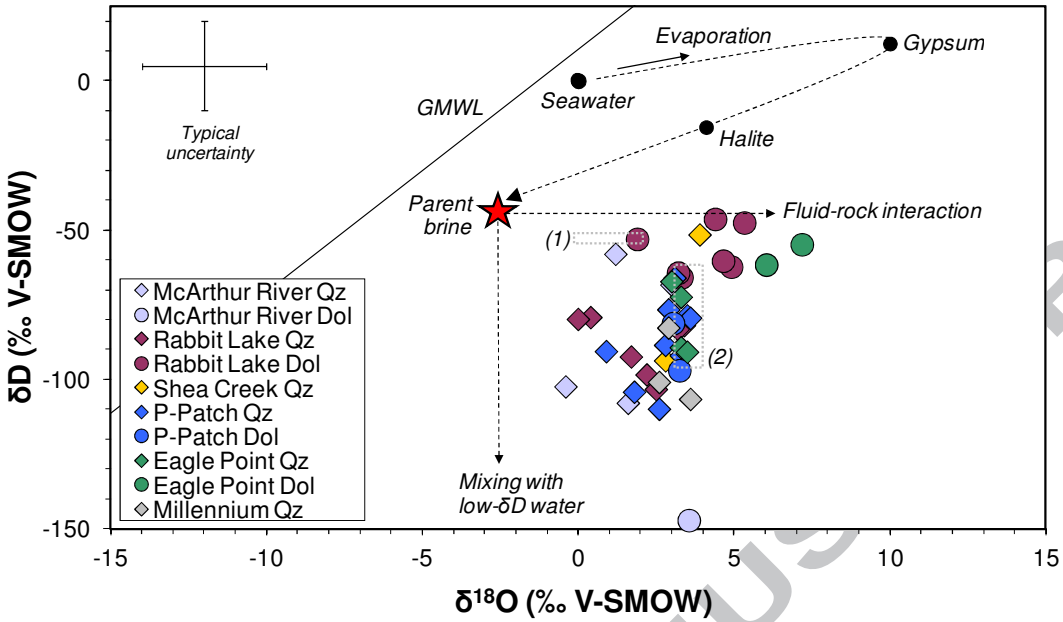


**FIGURE 6**

| Sample | Depth below U/C (m) | Description | Quartz veins | | Dolomite veins | | | |
|---|---|---|---|---|---|---|---|---|
| | | | Fluid inclusions | Quartz | Fluid inclusions | | Dolomite | |
| | | | $\delta D$ ($H_2O$) | $\delta^{18}O$ | $\delta D$ ($H_2O$) | $\delta^{13}C$ ($CO_2$) | $\delta^{18}O$ | $\delta^{13}C$ |
| *Eagle Point* | | | | | | | | |
| EPE44-17 | 13 | Qtz vein in fresh porphyry granite | | 16.2 | | | | |
| ES287-1 | 40 | Dol vein in fresh pelitic gneiss | | | -55 | -15 | 23.3 | -4.5 |
| DDH2306-1 | 130 | Qtz-sulfides vein in illitized pegm | -67 | 16.0 | | | | |
| DDH2306-2 | 135 | Qtz vein in illitized gneiss | | 16.8 | | | | |
| H1935-2 | 153 | Dol vein in chloritized pegm | | | | | 13.4 | -5.3 |
| H1935-4 | 159 | Hem-dol vein in hem-chl-rich pegm | | | | | 21.1 | -5.3 |
| H1935-5 | 159 | Qtz vein in hematized chloritized gneiss | | 16.4 | | | | |
| H1935-8 | 177 | Dol-hem vein in biotite-rich gneiss | | | -62 | -19 | 15.1 | -5.4 |
| DDH1733-14 | 179 | Qtz vein in bleached pegm | | 16.3 | | | | |
| EPE44-4 | 211 | Qtz vein in microgranite | | 16.0 | | | | |
| 287-14 | 248 | Qtz-dol vein in chloritized gneiss | | 15.3 | | | | |
| 287-8 | 253 | Qtz vein in bleached pelitic gneiss | | 16.1 | | | | |
| 287-10 | 259 | Qtz vein in bleached pelitic gneiss | -89 | 16.3 | | | | |
| EPE44-11 | 263 | Hem-dol vein in chloritized pegm | | | | | 17.3 | -11.2 |
| H3042-1 | 263 | Qtz-drv vein in graphite-rich gneiss | -72 | 16.3 | | | | |
| ES287-13 | 272 | Qtz cement in clay-hem-rich breccia | | 16.8 | | | | |
| EPE44-14 | 361 | Dol vein in chloritized pegm | | | | | 20.5 | -7.4 |
| ES287-23 | 429 | Qtz vein in hematized chloritized pegm | -91 | 16.5 | | | | |
| *McArthur River* | | | | | | | | |
| MAC48Qz | -42 | Qtz vein surrounding U ore | | 11.9 | | | | |
| MAC8Qz | sst | Qtz-sulfides vein in silicified sst | -68 | 16.0 | | | | |
| MAC13Qz | sst | Qtz-drv breccia in silicified sst | -102 | 12.6 | | | | |
| MAC5 | 25 | Qtz-Dol vein surrounding U ore | -58 | 14.2 | -147 | -30 | 19.7 | -23.5 |
| MAC54Qz | 50 | Qtz-drv-sulfides in chl-rich breccia | -108 | 14.6 | | | | |
| *Millennium* | | | | | | | | |
| CX52-1 | 99 | Qtz-dol vein in bleached gneiss | -107 | 16.6 | | | | |
| CX48-03 | 130 | Qtz-drv vein in bleached gneiss | -101 | 15.6 | | | | |
| CX44-2 | 213 | Qtz vein in fresh gneiss | -83 | 15.9 | | | | |
| CX48-01-12a | 265 | Qtz vein in hematized gneiss | | 17.4 | | | | |
| CX51 | bst | Qtz filling vugs in hem-ill-chl breccia | | 16.3 | | | | |
| *P-Patch* | | | | | | | | |
| P55-15 | 24 | Dol vein in chloritized gneiss | | | | | 23.5 | -9.4 |
| P48-1 | 29 | Qtz vein in chloritized gneiss | -79 | 16.5 | | | | |
| P48-2 | 39 | Qtz vein in chloritized gneiss | -79 | 16.6 | | | | |
| P48-3 | 40 | Qtz-dol vein in chloritized gneiss | -77 | 15.9 | -97 | -19 | 19.4 | -5.6 |
| P53-10 | 42 | Dol vein in fresh pelitic gneiss | | | | | 15.6 | -6.5 |
| P48-5 | 52 | Qtz vein in bleached gneiss | -66 | 16.1 | | | | |
| P54-5 | 64 | Qtz vein in fresh gneiss | -92 | 16.3 | | | | |
| P53-6 | 96 | Qtz vein in ill-chl-rich pegm | -110 | 15.6 | | | | |
| P63-6 | 104 | Massive dolomite with chl patches | | | -81 | -9 | 19.2 | -4.0 |
| P57-2 | 104 | Qtz vein in bleached pegm | -104 | 14.8 | | | | |
| P70-1 | 122 | Qtz-dol-hem-drv breccia | -89 | 15.8 | | | | |
| P49-4 | 149 | Dol vein in chloritized gneiss | | | | | 22.8 | -5.1 |
| P56-17 | 164 | Qtz-drv veins in ill-rich pelitic gneiss | -91 | 13.9 | | | | |
| *Rabbit Lake* | | | | | | | | |
| DDH197-2 | 21 | Qtz vein in gneiss | -82 | 16.4 | | | | |
| DDH7-1 | 125 | Qtz filling vugs in dequartzified gneiss | | 15.9 | | | | |
| DDH7-32-8 | 300 | Qtz filling vugs in dequartzified gneiss | | 15.0 | | | | |
| DDH197-5 | bst | Dol-chl vein in gneiss | | | -66 | -16 | 14.5 | -5.3 |
| RB3Qz1 | bst | Qtz cementing chl-drv breccia | | 15.5 | | | | |
| RBL11Carb | bst | Dol in bleached gneiss | | | -62 | -8 | 16.1 | -5.1 |
| RBL14 | bst | Qtz-dol vein in gneiss | -79 | 13.4 | -46 | -4 | 20.5 | -4.5 |
| RBL1 | bst | Qtz-dol vein in gneiss | | 13.6 | -48 | -11 | 16.6 | -4.9 |
| RBL2 | bst | Qtz-dol vein in hem-rich gneiss | -80 | 13.0 | -64 | -12 | 14.4 | -4.8 |
| RBL3Qz | bst | Qtz fragment in chl-drv breccia | -92 | 14.7 | | | | |
| RBL4Qz | bst | Qtz-dol vein in gneiss | | 16.5 | | | | |
| RBL5 | bst | Qtz-dol vein in hydraulic megabreccia | -98 | 15.2 | -53 | -12 | 13.1 | -6.6 |
| RBL7 | bst | Qtz-dol vein in hydraulic megabreccia | -103 | 15.5 | -60 | -16 | 15.9 | -5.0 |
| RBL9 | bst | Qtz-dol vein in gneiss | -83 | 16.2 | | | 13.7 | -6.3 |
| *Shea Creek* | | | | | | | | |
| SHE03 externe | sst | Qtz vein in bleached sst | | 16.7 | | | | |
| IF74 | sst | Qtz-drv breccia in sandsones | | 14.1 | | | | |
| SHE123-9-H503 | 50 | Qtz-drv veins in chloritized gneiss | | 12.9 | | | | |
| SHE123-9-H506 | 62 | Qtz-hem vein in bleached gneiss | -94 | 15.8 | | | | |
| SHE38a | 63 | Qtz vein in gneiss | | 15.4 | | | | |
| ERC5-922.0 | 195 | Qtz-hem vein in hematized gneiss | -52 | 16.9 | | | | |

**TABLE 1**

| | Detection | Analytical | *Eagle Point* | | *P-Patch* | | | | *Rabbit Lake* | | | | | | | | *McArthur River* |
|---|---|---|---|---|---|---|---|---|---|---|---|---|---|---|---|---|---|
| | limit | uncertainty | H1935-8 | ES287-1 | P48-3Dol | P53-10 | P55-15 | P63-6 | DDH197-5 | RBL11 | RBL14 | RBL1 | RBL2 | RBL5 | RBL7 | RBL9 | MAC5 |
| $SiO_2$ (wt.%) | 0.05 | 1-10% | 2.53 | 0.86 | 0.21 | 6.56 | 39.94 | 1.69 | *bdl* | 0.41 | *bdl* | 0.53 | 5.37 | *bdl* | *bdl* | 8.84 | 1.57 |
| $TiO_2$ | 0.005 | >25% | *bdl* | *bdl* | *bdl* | *bdl* | *bdl* | *bdl* | *bdl* | *bdl* | *bdl* | *bdl* | *bdl* | *bdl* | *bdl* | *bdl* | *bdl* |
| $Al_2O_3$ | 0.015 | 10-25% | 0.10 | 0.12 | *bdl* | 0.61 | *bdl* | 0.09 | 0.06 | *bdl* | *bdl* | *bdl* | *bdl* | *bdl* | *bdl* | *bdl* | *bdl* |
| $Fe_2O_3$ | 0.04 | 2-15% | 7.34 | 2.21 | 2.26 | 3.00 | 1.00 | 2.08 | 1.04 | 1.12 | 2.67 | 2.81 | 2.32 | 1.02 | 0.95 | 0.80 | 3.03 |
| MnO | 0.001 | 2-5% | 0.32 | 1.04 | 0.23 | 0.70 | 0.37 | 0.14 | 0.06 | 0.08 | 0.20 | 0.20 | 0.19 | 0.07 | 0.06 | 0.04 | 0.07 |
| MgO | 0.01 | <2% | 16.16 | 18.58 | 20.05 | 18.21 | 12.51 | 20.34 | 21.25 | 21.02 | 20.08 | 19.95 | 19.11 | 21.18 | 21.23 | 19.50 | 18.11 |
| CaO | 0.02 | <2% | 28.37 | 29.90 | 29.80 | 27.56 | 18.29 | 29.07 | 29.93 | 29.92 | 29.89 | 29.78 | 28.06 | 30.00 | 30.01 | 27.61 | 31.68 |
| $Na_2O$ | 0.07 | <15% | *bdl* | 0.08 | *bdl* | *bdl* | *bdl* | *bdl* | *bdl* | *bdl* | *bdl* | *bdl* | *bdl* | *bdl* | *bdl* | *bdl* | *bdl* |
| $K_2O$ | 0.05 | >25% | *bdl* | *bdl* | *bdl* | *bdl* | *bdl* | *bdl* | *bdl* | *bdl* | *bdl* | *bdl* | *bdl* | *bdl* | *bdl* | *bdl* | *bdl* |
| $P_2O_5$ | 0.015 | >25% | *bdl* | *bdl* | *bdl* | *bdl* | *bdl* | *bdl* | *bdl* | *bdl* | *bdl* | *bdl* | *bdl* | *bdl* | *bdl* | *bdl* | *bdl* |
| LOI | | | 44.09 | 45.71 | 46.47 | 42.76 | 28.67 | 45.70 | 46.31 | 46.28 | 46.38 | 45.79 | 44.10 | 46.51 | 46.50 | 42.45 | 44.59 |
| SUM | | | 98.92 | 98.50 | 99.01 | 99.45 | 100.78 | 99.10 | 98.64 | 98.82 | 99.21 | 99.06 | 99.14 | 98.78 | 98.74 | 99.25 | 99.05 |
| Mg/Ca (mol) | | | 0.82 | 0.89 | 0.97 | 0.95 | 0.98 | 1.00 | 1.02 | 1.01 | 0.96 | 0.96 | 0.98 | 1.01 | 1.02 | 1.01 | 0.82 |
| Cs (ppm) | 0.1 | 15-25% | *bdl* | *bdl* | *bdl* | *bdl* | *bdl* | *bdl* | *bdl* | *bdl* | *bdl* | *bdl* | *bdl* | *bdl* | *bdl* | *bdl* | *bdl* |
| Rb | 0.3 | 15-25% | 1.96 | 1.47 | *bdl* | 0.49 | *bdl* | *bdl* | *bdl* | *bdl* | *bdl* | *bdl* | *bdl* | *bdl* | *bdl* | *bdl* | *bdl* |
| Sr | 1.7 | 5-15% | 38.47 | 46.46 | 42.28 | 20.56 | 27.70 | 57.33 | 30.18 | 28.11 | 26.36 | 25.70 | 16.72 | 38.20 | 39.69 | 20.79 | 59.73 |
| Ba | 2 | 15-25% | 11.68 | 14.15 | *bdl* | 9.88 | 2.63 | *bdl* | *bdl* | *bdl* | *bdl* | *bdl* | *bdl* | *bdl* | *bdl* | 2.58 | *bdl* |
| Be | 0.2 | <15% | 1.82 | 1.03 | *bdl* | *bdl* | *bdl* | *bdl* | *bdl* | *bdl* | *bdl* | *bdl* | *bdl* | *bdl* | *bdl* | *bdl* | *bdl* |
| Y | 0.15 | <5% | 42.42 | 62.92 | 9.97 | 27.12 | 15.59 | 15.38 | 10.72 | 12.81 | 19.57 | 19.70 | 9.66 | 39.15 | 36.47 | 10.32 | *bdl* |
| Zr | 1.5 | >25% | *bdl* | *bdl* | 5.26 | 4.98 | *bdl* | *bdl* | *bdl* | *bdl* | *bdl* | *bdl* | *bdl* | *bdl* | *bdl* | *bdl* | *bdl* |
| Hf | 0.03 | >25% | 0.05 | 0.04 | 0.03 | 0.11 | *bdl* | *bdl* | 0.03 | *bdl* | *bdl* | *bdl* | *bdl* | *bdl* | *bdl* | *bdl* | *bdl* |
| Nb | 0.07 | <15% | 0.43 | 0.14 | 0.32 | 0.11 | *bdl* | 0.10 | 0.13 | *bdl* | *bdl* | *bdl* | *bdl* | *bdl* | *bdl* | *bdl* | 0.19 |
| Ta | 0.01 | >25% | 0.07 | 0.04 | 0.05 | 0.02 | *bdl* | 0.02 | 0.01 | 0.02 | 0.02 | *bdl* | 0.02 | 0.02 | 0.01 | *bdl* | 0.02 |
| Th | 0.05 | 15-25% | 0.21 | 0.06 | 0.06 | 0.08 | 0.20 | 0.57 | 0.10 | 0.07 | 0.06 | 0.12 | 0.09 | *bdl* | *bdl* | *bdl* | *bdl* |
| U | 0.05 | <8% | 0.41 | 0.87 | 152.50 | 0.31 | 3.04 | 0.99 | 0.35 | 1.59 | 0.62 | 0.16 | 0.34 | 12.91 | 12.78 | 0.56 | 16.35 |
| Pb | 0.9 | 5-10% | 1.07 | *bdl* | 2.06 | 1.20 | 4.48 | 4.04 | *bdl* | *bdl* | 2.18 | *bdl* | *bdl* | 1.38 | 1.55 | *bdl* | 81.65 |
| V | 0.6 | 10-25% | 3.69 | 1.90 | 2.09 | 1.96 | 3.10 | 6.17 | 19.62 | 27.14 | 15.31 | 32.29 | 13.21 | 5.22 | 4.50 | 4.67 | 2.14 |
| Ni | 2 | 5-25% | *bdl* | *bdl* | 8.10 | 8.38 | 7.20 | 5.12 | *bdl* | 5.96 | 6.72 | *bdl* | 5.96 | 5.20 | 5.07 | 6.66 | 117.70 |
| Cr | 3 | >25% | *bdl* | *bdl* | *bdl* | *bdl* | *bdl* | *bdl* | *bdl* | *bdl* | *bdl* | *bdl* | *bdl* | *bdl* | *bdl* | *bdl* | *bdl* |
| Mo | 0.4 | 5-25% | *bdl* | *bdl* | *bdl* | *bdl* | 2.09 | *bdl* | *bdl* | 1.53 | *bdl* | *bdl* | *bdl* | *bdl* | *bdl* | 0.48 | 75.81 |
| Co | 0.5 | 5-25% | 0.86 | 0.63 | 1.60 | 3.25 | 3.43 | 3.86 | 1.12 | 3.04 | 7.98 | 2.91 | 6.31 | 2.03 | 2.66 | 1.52 | 92.75 |
| Cu | 3 | 5-25% | *bdl* | 11.75 | 139.50 | 15.80 | 30.59 | 7.56 | 22.42 | *bdl* | 10.06 | *bdl* | 316.60 | 125.80 | 93.60 | 7.65 | 22.36 |
| Zn | 6 | <15% | *bdl* | *bdl* | *bdl* | *bdl* | *bdl* | *bdl* | 34.83 | *bdl* | *bdl* | *bdl* | *bdl* | *bdl* | *bdl* | *bdl* | *bdl* |
| Cd | 0.15 | >25% | *bdl* | *bdl* | *bdl* | *bdl* | *bdl* | *bdl* | *bdl* | *bdl* | *bdl* | *bdl* | *bdl* | *bdl* | *bdl* | *bdl* | *bdl* |
| Ga | 0.1 | 8-25% | 0.64 | 1.49 | *bdl* | 1.57 | 0.37 | *bdl* | 0.31 | 0.48 | *bdl* | *bdl* | *bdl* | *bdl* | *bdl* | *bdl* | *bdl* |
| In | 0.06 | 5-15% | *bdl* | *bdl* | 0.37 | *bdl* | 0.18 | 0.34 | 0.17 | 0.76 | 0.85 | 1.13 | 0.58 | *bdl* | *bdl* | *bdl* | *bdl* |
| Ge | 0.05 | 5-15% | 0.13 | 0.17 | *bdl* | 0.17 | 0.37 | 0.14 | *bdl* | *bdl* | *bdl* | *bdl* | 0.13 | *bdl* | *bdl* | 0.18 | *bdl* |
| As | 1.8 | 5-15% | *bdl* | *bdl* | 8.45 | 2.53 | 4.38 | 6.22 | *bdl* | *bdl* | *bdl* | *bdl* | *bdl* | *bdl* | *bdl* | *bdl* | 3.95 |
| Bi | 0.1 | 5-15% | *bdl* | *bdl* | 0.10 | 0.15 | 1.65 | 1.17 | *bdl* | 1.32 | *bdl* | *bdl* | *bdl* | *bdl* | 0.14 | 0.11 | 0.44 |
| Sb | 0.1 | >25% | *bdl* | *bdl* | *bdl* | *bdl* | *bdl* | *bdl* | *bdl* | *bdl* | *bdl* | *bdl* | *bdl* | *bdl* | *bdl* | *bdl* | *bdl* |
| Sn | 0.2 | >25% | *bdl* | *bdl* | 0.65 | *bdl* | 0.56 | 0.69 | *bdl* | *bdl* | *bdl* | *bdl* | *bdl* | *bdl* | *bdl* | *bdl* | *bdl* |
| W | 0.15 | >25% | *bdl* | *bdl* | 0.35 | *bdl* | *bdl* | 0.50 | *bdl* | *bdl* | *bdl* | *bdl* | *bdl* | *bdl* | *bdl* | *bdl* | *bdl* |
| La | 0.07 | <5% | 29.83 | 77.82 | 1.71 | 16.51 | 1.99 | 1.21 | 0.77 | 0.93 | 0.73 | 0.33 | 0.38 | 2.00 | 2.11 | 0.78 | 1.77 |
| Ce | 0.12 | 5-25% | 53.18 | 153.00 | 6.12 | 30.77 | 6.74 | 4.58 | 2.87 | 3.61 | 3.73 | 1.94 | 1.47 | 13.47 | 14.19 | 2.32 | 0.31 |
| Pr | 0.01 | 5-25% | 6.21 | 16.59 | 1.00 | 3.84 | 1.17 | 0.77 | 0.43 | 0.59 | 0.67 | 0.37 | 0.26 | 2.64 | 2.68 | 0.31 | 0.03 |
| Nd | 0.06 | 5-20% | 24.57 | 59.24 | 4.73 | 16.24 | 5.77 | 3.80 | 1.85 | 2.62 | 2.94 | 1.70 | 1.20 | 12.34 | 12.34 | 1.28 | 0.08 |
| Sm | 0.015 | 5-10% | 5.55 | 10.80 | 2.30 | 4.21 | 2.81 | 1.88 | 0.65 | 0.88 | 1.51 | 1.10 | 0.67 | 4.21 | 4.12 | 0.41 | *bdl* |
| Eu | 0.005 | 5-25% | 1.51 | 5.02 | 0.87 | 1.48 | 0.59 | 0.58 | 0.18 | 0.27 | 0.45 | 0.36 | 0.21 | 1.17 | 1.10 | 0.10 | 0.01 |
| Gd | 0.01 | <5% | 6.37 | 9.26 | 2.81 | 4.21 | 3.55 | 3.06 | 1.01 | 1.33 | 3.14 | 2.74 | 1.45 | 4.92 | 4.70 | 0.68 | *bdl* |
| Tb | 0.005 | <5% | 1.01 | 1.43 | 0.44 | 0.65 | 0.58 | 0.55 | 0.28 | 0.36 | 0.76 | 0.74 | 0.36 | 1.28 | 1.21 | 0.22 | *bdl* |
| Dy | 0.01 | 5-15% | 5.98 | 8.75 | 2.10 | 3.95 | 2.89 | 2.89 | 1.98 | 2.53 | 4.23 | 4.32 | 2.07 | 8.26 | 7.78 | 1.73 | 0.01 |
| Ho | 0.005 | 5-15% | 1.17 | 1.77 | 0.31 | 0.79 | 0.48 | 0.49 | 0.33 | 0.41 | 0.65 | 0.66 | 0.32 | 1.27 | 1.17 | 0.33 | *bdl* |
| Er | 0.005 | 5-15% | 3.12 | 5.02 | 0.76 | 2.32 | 1.14 | 1.18 | 0.82 | 1.02 | 1.49 | 1.52 | 0.78 | 2.91 | 2.72 | 0.87 | 0.01 |
| Tm | 0.005 | 5-25% | 0.43 | 0.74 | 0.11 | 0.38 | 0.16 | 0.17 | 0.11 | 0.14 | 0.21 | 0.21 | 0.11 | 0.40 | 0.38 | 0.13 | *bdl* |
| Yb | 0.005 | 5-25% | 2.68 | 5.11 | 0.82 | 2.77 | 1.11 | 1.20 | 0.68 | 1.03 | 1.48 | 1.41 | 0.81 | 2.85 | 2.59 | 0.85 | 0.01 |
| Lu | 0.005 | <5% | 0.41 | 0.78 | 0.13 | 0.45 | 0.16 | 0.18 | 0.10 | 0.16 | 0.21 | 0.20 | 0.12 | 0.42 | 0.39 | 0.13 | *bdl* |

**TABLE 2**

| Sample | Rb ppm | Sr ppm | $^{87}Sr/^{86}Sr \pm 2\sigma$ | $(^{87}Rb/^{86}Sr)$ | $(^{87}Sr/^{86}Sr)_i$ | Sm ppm | Nd ppm | $^{147}Sm/^{144}Nd$ | $^{143}Nd/^{144}Nd \pm 2\sigma$ | $\varepsilon_{Nd}(t)$ |
|---|---|---|---|---|---|---|---|---|---|---|
| *Eagle Point* | | | | | | | | | | |
| H1935-8 | 2.0 | 38.5 | 0.718747 ± 0.00001 | 0.1471 | 0.7161 ± 0.0005 | 5.6 | 24.6 | 0.1366 | 0.511542 ± 0.000007 | -11.8 ± 1.9 |
| ES287-1 | 1.5 | 46.5 | 0.711050 ± 0.00001 | 0.0917 | 0.7094 ± 0.0003 | 10.8 | 59.2 | 0.1102 | 0.511253 ± 0.000006 | -13.2 ± 2.8 |
| *P-Patch* | | | | | | | | | | |
| P48-3 | < 0.3 | 42.3 | 0.707945 ± 0.00001 | 0.0103 | | 2.3 | 4.7 | 0.2940 | 0.512398 ± 0.000010 | -20.3 ± 3.2 |
| P53-10 | 0.5 | 20.6 | 0.709526 ± 0.00001 | 0.0694 | 0.7083 ± 0.0002 | 4.2 | 16.2 | 0.1568 | 0.511391 ± 0.000005 | -18.0 ± 1.3 |
| P55-15 | < 0.3 | 27.7 | 0.710542 ± 0.00001 | 0.0157 | | 2.8 | 5.8 | 0.2938 | 0.512251 ± 0.000012 | -23.2 ± 3.2 |
| P63-6 | < 0.3 | 57.3 | 0.708407 ± 0.00001 | 0.0076 | | 1.9 | 3.8 | 0.2993 | 0.512491 ± 0.000010 | -19.3 ± 3.3 |
| *Rabbit Lake* | | | | | | | | | | |
| DDH197-5 | < 0.3 | 30.2 | 0.705622 ± 0.00001 | 0.0144 | | 0.6 | 1.8 | 0.2110 | 0.512206 ± 0.000012 | -10.7 ± 0.5 |
| RBL11 | < 0.3 | 28.1 | 0.707559 ± 0.00001 | 0.0154 | | 0.9 | 2.6 | 0.2020 | 0.512231 ± 0.000017 | -8.8 ± 0.2 |
| RBL14 | < 0.3 | 26.4 | 0.707166 ± 0.00001 | 0.0165 | | 1.5 | 2.9 | 0.3111 | 0.512810 ± 0.000016 | -15.0 ± 3.7 |
| RBL1 | < 0.3 | 25.7 | 0.706697 ± 0.00001 | 0.0169 | | 1.1 | 1.7 | 0.3923 | 0.513774 ± 0.000030 | -9.2 ± 6.3 |
| RBL2 | < 0.3 | 16.7 | 0.706810 ± 0.00001 | 0.0260 | | 0.7 | 1.2 | 0.3372 | 0.513047 ± 0.000010 | -14.6 ± 4.5 |
| RBL5 | < 0.3 | 38.2 | 0.705296 ± 0.00001 | 0.0114 | | 4.2 | 12.3 | 0.2063 | 0.512138 ± 0.000007 | -11.3 ± 0.3 |
| RBL7 | < 0.3 | 39.7 | 0.705418 ± 0.00001 | 0.0109 | | 4.1 | 12.3 | 0.2016 | 0.512152 ± 0.000007 | -10.3 ± 0.2 |
| RBL9 | < 0.3 | 20.8 | 0.705751 ± 0.00001 | 0.0209 | | 0.4 | 1.3 | 0.1925 | 0.512062 ± 0.000013 | -10.6 ± 0.1 |
| *McArthur River* | | | | | | | | | | |
| MAC5 | < 0.3 | 59.7 | 0.709962 ± 0.00001 | 0.0073 | 0.7100 ± 0.0002 | 0.01 | 0.1 | | | |

**TABLE 3**